university of groningen / faculty of science and engineering / mathematics and applied mathematics

Complex Dynamics of Magnetic Billiards in a 2-Torus

Master Project Mathematics

October 2023

Student: A. Silvans

First supervisor: Prof. dr. M. Seri

Second supervisor: Dr. H. Jardón-Kojakhmetov

Abstract

The study of mathematical billiards is a prominent topic within dynamical systems. One of the most important examples of a billiard is the Sinai billiard: a single particle on a 2-torus with a circular obstacle, if the particle collides with the boundary of the obstacle, it does so elastically. Once the particle is set in motion, its long term behavior is studied: is the motion ergodic, do there exist periodic trajectories? Other such billiards can be devised, and for each we can expect its own challenge.

We consider a variation of the Sinai billiard where the solid boundary is removed and in the interior of the disc there is a magnetic field. Now, the particle passes through and its trajectory is deflected. This introduces a parameter, the magnetic field strength, which we can vary, and study.

We approach the magnetic Sinai billiard from two perspectives. First, we consider it in the context of KAM theory, which deals with Hamiltonian systems and small perturbations. Next, we study the system using symbolic dynamics, more specifically, we use the Lempel-Ziv complexity to distinguish initial conditions that lead to ordered dynamics from those that lead to disorder. In such a way, we characterize qualitatively different dynamics of the system.

Contents

1 Introduction **4**

2 Prelimiaries and basic properties **7**
2.1 Equations of motion of the magnetic Sinai billiard 7
2.2 KAM theory 9
2.3 Approximating locally L^1 functions 10
2.4 Poincaré sections and stability of maps 11
2.5 Symbolic dynamics and semi-conjugacy 15
2.6 The Lempel-Ziv compression algorithm 16

3 Weak magnetic fields and KAM theory **18**
3.1 Investigating small magnetic field strengths 18
3.2 Perturbations of linear motion 19
3.3 Perturbation of motion in a constant field 19

4 Complexity and symbolic dynamics **22**
4.1 First periodic trajectories and stability analysis 22
4.2 Symbolic dynamics of the magnetic Sinai billiard 24
4.3 Lempel-Ziv varying b and initial conditions 25
4.4 Lempel-Ziv Poincaré sections for fixed b 28
4.5 Checking for quasi-periodicity 30

5 Conclusion **33**
5.1 Further questions 34
5.2 Acknowledgements 35

List of Figures

1 Comparing a Lorentz gas and a magnetic Lorentz gas. 4
2 Motivating example for the use of KAM theory. 18
3 Numerical analysis of the fitting of $\hat{b} = \pi R^2 b$ 20
4 Stable trajectories discovered analytically. 23
5 Unstable trajectories discovered analytically. 24
6 LZC for a 2 parameter family of initial conditions 26
7 Zooming in for more detail in the 2 parameter family plot 26
8 Fractal-like structure arising from LZC 27
9 LZC plot of a few Poincaré sections 28
10 Another LZC plot of a few Poincaré sections 29
11 First signs of intricate quasi-periodicity. 30
12 Complex and ornamental quasi-periodic trajectories. 30
13 A symmetry breaking trajectory and an honorable mention. . . . 31
14 Wandering in $\mathbb{R}^2$, yet quasi-periodic in $\mathbb{T}^2$. 31
15 Evidence supporting the claims for small b values 32
16 Motivating example for Levy flight interpretation 35

1 Introduction

In the theory of mathematical billiards, a particle, much like a billiard ball, is set in motion on a "table". The table may have walls or obstructions or there may be regions where the velocity of the particle is deflected in some way. The table need not be flat, and can seem entirely unrealistic. The goal of the game in our case is to characterize the long term behavior of the particle as it travels on the table.

The study of mathematical billiards can be traced back to Boltzmann's ergodic hypothesis in statistical mechanics. The question at its simplest was: do gas particles trapped in a box behave stochastically? That is, can we determine whether the motion of these particles is truly random? This was modeled with the *Sinai billiard* [Sin63], a particular instance of a *Lorentz gas*, and determined to be true. The Sinai billiard is a billiard on a 2-torus $\mathbb{T}^2 = \mathbb{R}^2/\mathbb{Z}^2$ with a disc shaped wall on it, an example can be found in fig. 1a, where the torus is unfolded on the plane, and the system is viewed as a periodic Lorentz gas. The particle travels along a straight path on $\mathbb{T}^2$ and is elastically reflected when it hits the boundary of the disc.

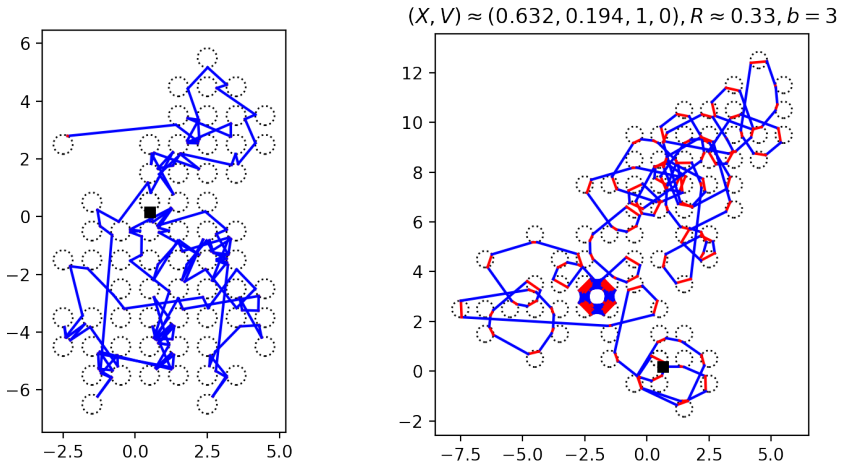

(a) A particle in a periodic Lorentz gas.

(b) A particle in a periodic magnetic Lorentz gas.

Figure 1: Unlike a classical Lorentz gas with elastic reflection, a particle in a magnetic one experiences a translation along the boundary of the discs together with the elastic reflection. Hence, introducing a new variable for study.

In this thesis we consider a variation of this problem which we call a *magnetic billiard*, where instead of a solid disc, we have a magnetic bump. When the space the particle travels in is $\mathbb{R}^2$ with circular obstacles, the system is called a Lorentz gas, while when the space is $\mathbb{T}^2$, it is a Sinai billiard. We study the magentic Sinai billiard but find it useful to also consider the periodic magnetic Lorentz gas, since they are related by unfolding the 2-torus. In fig. 1b we demonstrate the types of motion exhibited by a trajectory of a particle in a magnetic Lorentz gas. In blue we indicate free motion, and in red we have motion within the

magnetic field, the black square is the initial position. The red segments should instead be circular arcs, we reserve some artistic liberty in this choice. There is a magnetic disc at every point in the lattice $\mathbb{Z}^2 + 1/2$ but we only draw the boundary of the discs that are hit by the particle, and skip the rest to improve legibility. More precisely, we study the dynamics arising from the magnetic Hamiltonian $H : \mathbb{R}^3 \times \mathbb{R}^3 \to \mathbb{R}$:

$$H(q,p) = \frac{1}{2}\|p - A(q)\|^2 \tag{1}$$

where $q = (q_1, q_2, q_3)$ is position, $p = (p_1, p_2, p_3)$ is momentum, and $A : \mathbb{R}^3 \to \mathbb{R}^3$ is a magnetic vector potential defined as follows:

$$A(q) = \begin{cases} (-bq_2, 0, 0), & \text{if } (q_1, q_2) \in S, \\ (0,0,0), & \text{if } (q_1, q_2) \in [0,1]^2 \backslash S, \\ A(q \bmod 1), & \text{otherwise,} \end{cases}$$

where $S = \{x \in \mathbb{R}^2 : \|x - 1/2\| \leq R\}$ is a disc centered at $(1/2, 1/2)$ with radius $R \in (0, 1/2)$ and $b \in (0, \infty)$ is the magnetic field strength. We finish formally introducing the system in the preliminaries.

Similar problems have been considered before in [KS17] and [Gas21]. In the former, the dynamics of a particle in the plane with finitely many magnetic bumps was considered and this was studied using symbolic dynamics. In the latter, we see *inverse* magnetic billiards, where the particle experiences a magnetic field in the space surrounding the bumps and free motion within the bumps, such a system gives rise to interesting periodic behavior. We take inspiration from these works, and use techniques in symbolic dynamics and also study periodic trajectories that arise from the system in question.

More generally, billiards for a wide range of potentials have been considered, as in [DL91], where several classes of radially symmetric potentials are studied and conditions for ergodicity are given. Similar systems are considered in applications as well, for example in the study of quantum dots and magnetic quantum dots [LSIC04], which model particle and field interaction in spintronic materials. Hence, understanding the dynamics of (1) more deeply has practical interest as well.

Focusing on the behavior of the trajectory in fig. 1b, we see:

- erratic behavior, that is, the trajectory seems to bounce around in a chaotic manner;
- evidence for existence of trapped quasi-periodic motion, specifically referring to the spot where the particle is trapped between four discs before eventually escaping;
- two distinct scales, the intervals of magnetic motion serve as a perturbation or deflection and are rather local, while the intervals of free motion can be long and in fact can be arbitrarily long provided that the particle exits a disc at a shallow enough angle.

We see that the motion is not trivial, and warrants study. What is not yet evident from fig. 1b is the influence of the parameters R and b on the general

behavior of the system. This is what we aim to better understand by the end of the thesis.

We outline how we study this system. We focus on varying b, and identify three modes. For some $b_1, b_2 \in \mathbb{R}$ with $0 < b_1 \ll 1/R < b_2$,

1. If $0 < b < b_1$, the field strength is weak. We can use KAM theory to make sense of quasi-periodicity at these strengths. We find that we may consider our system as a perturbation of either free motion, or the flow of a uniform magnetic field in the plane.

2. If $b_1 < b < b_2$, the field has moderate strength and new dynamics of varying complexity start appearing. We study this mode, using symbolic dynamics and the Lempel-Ziv complexity.

There is also the strong field case $b > b_2$ which is also interesting to consider but will not be treated here. We expect in this case to see disorganised, possibly ergodic in $\mathbb{T}^2$, motion almost everywhere. This can be motivated by considering the limit as $b \to \infty$, the magnetic deflection of (1) tends to elastic collision, so the motion is comparable to the Sinai billiard which we know to be ergodic.

To aid in the exploration, a large component of our work is numerical analysis and the use of symbolic algebra systems. We primarily use the tools provided by the `Python` language, specifically, we use existing tools such as `NumPy`, `SymPy`, and `Matplotlib`. We also wrote our own module `magdynsys.py` for computing and visualizing data. Our material is available online [Sil23], along with all the figures we made and the `Jupyter` notebooks we created.

2 Prelimiaries and basic properties

2.1 Equations of motion of the magnetic Sinai billiard

We first define the Hamiltonian equation of a magnetic vector potential A, and some related concepts. We then solve for the equations of motion for a specific choice of vector field. We follow the description of a magnetic Hamiltonian as in [Ser22]. Let $H : \mathbb{R}^3 \times \mathbb{R}^3 \to \mathbb{R}$ be a magnetic Hamiltonian function:

$$H(q,p) = \frac{1}{2m}\left\|p - \frac{e}{c}A(q)\right\|^2$$

as before $A : \mathbb{R}^3 \to \mathbb{R}^3$ is a magnetic vector potential, we also have mass m, the charge of a point particle e, and the speed of light in a vacuum c. In our discussions, the physical constants are not important, so we set $m = e = c = 1$. Equivalently, p and A can be scaled to compensate the contribution of m, c, and e. The *magnetic vector field* is defined as $B = \operatorname{curl} A = \nabla \times A$. The magnetic field B is a physical quantity, when visualizing, we typically draw the *field lines*, that is, we draw the curves that indicate the direction of B. The potential A is a more abstract notion, and we have some freedom in its choice. To define a system, we first consider the field B we want to study, and then to construct a Hamiltonian H which governs the motion due to B, we choose a potential A such that $B = \operatorname{curl} A$. There is freedom in choosing A, since picking any twice differentiable $f : \mathbb{R}^3 \to \mathbb{R}$, we see that $\operatorname{curl}(A + \operatorname{div} f) = \operatorname{curl} A$ by the result: $\nabla \times (\nabla f) = 0$. Lastly, since H does not depend explicitly on time, it is constant on its trajectories, and the subspaces $\{(q,p) \in \mathbb{R}^3 \times \mathbb{R}^3 : H(q,p) = E\}$ for $E \in \mathbb{R}$ are invariant subspaces of the motion.

Another important quantity we will use is the *flux* $\Phi_B(U)$ of the normal component of a magnetic field B through a surface U, defined as

$$\Phi_B(U) = \iint_U B \cdot dS,$$

where dS is the surface area form on U. An important result to mention is that the quantity $\Phi_B(U)$ depends solely on the geometry of the boundary ∂U. This is true by Stokes' theorem:

$$\Phi_B(U) = \iint_U \nabla \times A \cdot dS = \int_{\partial U} A \cdot d\Gamma,$$

where Γ is a parametrization of ∂U consistent with the orientation of U. The value of $\Phi_B(U)$ should be the same for any choice of A, so only ∂U decided the value. In particular, when ∂U is empty, that is, when U is a surface with no boundary, Stokes' theorem states that $\Phi_B(U) = 0$.

One of the simplest non-trivial vector fields B we can consider, and the one we use throughout the thesis is $B = (0, 0, b)$ for $b \in (0, \infty)$. We see B is uniformly constant and points in the positive q_3-direction. We call the parameter b the *field strength*. It is readily verified that we can pick $A = (-bq_2, 0, 0)$ as a vector potential, and the flux for a surface U contained in the q_1q_2-plane is $\Phi_B(U) = b\mathrm{Vol}(U)$ where $\mathrm{Vol}(U)$ is the area of U.

Let us now determine the equations of motion of $H(q,p)$ given our choice of potential A. So, explicitly, H is as follows:

$$H(q,p) = \frac{1}{2}(p_1 + bq_2)^2 + \frac{1}{2}p_2^2.$$

The equations of motion are the solution of the system of differential equations:

$$\dot{q} = \frac{\partial H}{\partial p}, \qquad \dot{p} = -\frac{\partial H}{\partial q},$$

where $\dot{q}, \dot{p}$ are derivatives with respect to time. Explicitly, we get:

$$\begin{aligned} \dot{q}_1 &= p_1 + bq_2 & \dot{p}_1 &= 0 \\ \dot{q}_2 &= p_2 & \dot{p}_2 &= -b(p_1 + bq_2) \\ \dot{q}_3 &= 0 & \dot{p}_3 &= 0. \end{aligned}$$

Notice how the equations for $\dot{q}_1, \dot{q}_2, \dot{p}_1, \dot{p}_2$ are independent of q_3, and p_3, hence if we take initial conditions $q_3 = p_3 = 0$, the motion will be restricted to the q_1q_2-plane. So, we can ignore q_3 altogether. Next, we can simplify the system further by noticing:

$$\ddot{q}_1 = b\dot{q}_2, \qquad \ddot{q}_2 = -b\dot{q}_1,$$

which is a system of coupled harmonic oscillators which we know how to solve. We provide the answer and skip further computations:

$$\begin{aligned} q_1(t) &= q_1(0) + \frac{p_2(0)}{b} + \rho \sin(\omega t + \varphi), \\ q_2(t) &= q_2(0) - \frac{p_1(0)}{b} + \rho \cos(\omega t + \varphi), \end{aligned}$$

where $\rho, \varphi \in \mathbb{R}$ are integration constants. Commonly, ω is called the *Larmor* frequency, it can be shown in the case at hand that $\omega = b$. By association we will also call ρ the *Larmor radius*. We see now that a particle in the field B will trace a circle of radius ρ centered at the point $(q_1(0) + p_2(0)/b, q_2(0) - p_1(0)/b) \in \mathbb{R}^2$. We also see that the Larmor radius satisfies:

$$\rho = \frac{\|(q_1(t), q_2(t))\|}{b} = \frac{2H(q_1(0), q_2(0))}{b},$$

that is, ρ relates to b and the value of H, which is constant for a particular solution of the equations of motion of H. Hence, for the rest of the thesis we restrict $H = 1/2$, so that the Larmor radius is given by $\rho = 1/b$.

Coming back to the magnetic potential defined in (1), that is,

$$A(q) = \begin{cases} (-bq_2, 0, 0), & \text{if } (q_1, q_2) \in S, \\ (0, 0, 0), & \text{if } (q_1, q_2) \in [0,1]^2 \backslash S, \\ A(q \bmod 1), & \text{otherwise,} \end{cases}$$

Where $S = \{x \in \mathbb{R}^2 : \|x - 1/2\| \leq R\}$ is a disc centered at $(1/2, 1/2)$ with radius $R \in (0, 1/2)$. We now know that if $(q_1, q_2) \in S$, then the trajectory follows a circular arc as described above. In the second case, there is no magnetic field, so the trajectory is in free motion, that is, it is a straight line. The last condition simply states that we tile S over the lattice $\mathbb{Z}^2 + 1/2$. This also means that we can consider H on the 2-torus $\mathbb{T}^2 = \mathbb{R}^2/\mathbb{Z}^2$ via the quotient $\pi : \mathbb{R}^2 \to \mathbb{T}^2$ with $\pi(x) = x \bmod 1$ where the mod function is applied entry-wise. We will refer to H on either surfaces $\mathbb{R}^2$ or $\mathbb{T}^2$ interchangeably, since visualization is sometimes

easier on $\mathbb{R}^2$ while certain theory is applicable only on $\mathbb{T}^2$. Likewise, we use S to refer to the lattice of discs on $\mathbb{Z}^2 + 1/2$ and the one disc in $\mathbb{T}^2$, and make it clear which we are referring to on a case by case basis.

The motion of a particle under H in the interior and exterior of S is now clear. However, we notice that A is discontinuous on ∂S. This is an issue when a trajectory enters S tangentially, when this happens the solution is not necessarily unique. Luckily, the set ∂S has measure zero, so its contribution to our analysis is negligible. In what follows, we assume that trajectories tangential to ∂S are in free motion. Now, the motion of (1) is completely determined.

2.2 KAM theory

We begin by recalling Kolmogorov-Arnold-Moser (KAM) theory, state one of the main KAM theorems, and briefly outline the main points of the theory. We refer the reader to [Kna18] for a more detailed account. We strongly recommend [Pö82] for reference, as it presents the version of the KAM theorem we use here.

KAM theory is a method for studying perturbations of integrable Hamiltonian systems. Its origins lie in Celestial and Hamiltonian mechanics, where it was used to study the orbits of planets. We denote by $H^0(q,p)$ an integrable Hamiltonian and by $H^1(q,p,\varepsilon)$ a perturbation, where $\varepsilon > 0$ is a small parameter.

Focusing on the integrable case, it is known by the Liouville-Arnold theorem that there exist *action-angle* coordinates, p, and q, respectively, so $H^0 := H^0(p)$ can be expressed in terms of the action variable only. The equations of motion in action-angle coordinates are given by:

$$\dot{q} = \omega, \qquad \dot{p} = 0,$$

where $\omega = \partial_p H^0(p)$, and $\partial_p H^0 : I \to \Omega \subseteq \mathbb{R}^n$ is the *frequency map*. It is called the frequency map, since in action-angle coordinates, the phase-space becomes $\mathbb{T}^n \times I$ where $I \subseteq \mathbb{R}^n$, and the dynamics of the system are completely expressed as rotations on an n-torus. More generally, this is only true for integrable systems with compact Lagrangian subspaces. Recall, that for fixed values of H, trajectories of the system lie on invariant subspaces, in fact, phase-space is foliated by a family of invariant tori $\mathbb{T}^n \times \{p\}$ for each $p \in I \subseteq \mathbb{R}^n$. We consider only integrable Hamiltonians with a *non-degenerate* frequency map, that is, $\det \partial_p^2 H^0 \neq 0$. Now, KAM theory deals with Hamiltonians of the form

$$H(q,p) = H^0(p) + \varepsilon H^1(q,p,\varepsilon),$$

where $0 < \varepsilon \ll 1$ is considered small, H^0 is the integrable part and H^1 is the perturbation. We can also define H for $q \in \mathbb{R}^n$ instead but make sure H is 2π-periodic in the position coordinates:

$$H(q + 2\pi, p) = H(q,p), \quad \text{for all } (q,p) \in \mathbb{R}^n \times I,$$

so that we can quotient $\mathbb{R}^n$ to a torus $\mathbb{T}^n$. What KAM theory ensures is that under the correct conditions, a "large" subset $\Omega_{\gamma,\tau} \subseteq \Omega$, with $\gamma, \tau > 0$ of invariant tori of $H^0(p)$ are preserved, though possibly deformed, under the perturbation H^1. The set $\Omega_{\gamma,\tau}$ is given by:

$$\Omega_{\gamma,\tau} = \bigcap_{\substack{k \in \mathbb{Z} \\ k \neq 0}} \left\{ \omega \in \Omega : |\omega \cdot k| \geq \gamma |k|^{-\tau} \right\}. \tag{2}$$

The condition for $\Omega_{\gamma,\tau}$ is called the *Diophantine condition*. It can be shown for $\tau > n-1$ that for almost all $x \in \mathbb{R}^n$ there exists a $\gamma > 0$ such that $x \in \Omega_{\gamma,\tau}$, so in particular, we can find $\gamma > 0$ so that a point $\omega \in \Omega$ satisfies $\omega \in \Omega_{\gamma,\tau}$. We finally consider the *Cantor* set

$$\hat{\Omega}_{\gamma,\tau} = \Omega_{\gamma,\tau} \cap \{\omega \in \Omega : d(\omega, \partial\Omega) \geq \gamma\},$$

that is, we remove points in $\Omega_{\gamma,\tau}$ that have distance less than γ from the boundary of Ω. It can be shown that $\Omega \backslash \bigcup_{\gamma>0} \hat{\Omega}_{\gamma,\tau}$ is a set of measure zero, so the measure of $\hat{\Omega}_{\gamma,\tau}$ becomes large for small γ, justifying the term "large". We can now give the KAM theorem as stated in [Pö82].

Theorem 1 (KAM Theorem)**.** Let the integrable Hamiltonian $H^0 : \mathbb{T}^n \times I \to \mathbb{R}$ be real analytic and non-degenerate, such that the frequency map $\partial_p H^0 : I \to \Omega$ is a diffeomorphism and let the perturbed Hamiltonian $H = H^0 + \varepsilon H^1$ be of class $C^{\alpha\lambda+\lambda+\tau}$ with $\lambda > \tau + 1 > n$ and $\alpha > 1$. Then there exists a positive γ-independent δ such that for $|\varepsilon| < \gamma^2\delta$ with γ sufficiently small, there exists a diffeomorphism

$$\mathcal{T} : \mathbb{T}^n \times \Omega \to \mathbb{T}^n \times I,$$

which on $\mathbb{T}^n \times \hat{\Omega}_{\gamma,\tau}$ transforms the equations of motion of H into

$$\dot{\theta} = \omega, \qquad \dot{\omega} = 0.$$

The map $\mathcal{T}$ is of class C^α for non-integer α.

So, for $\omega \in \hat{\Omega}_{\gamma,\tau}$, we parametrize an invariant torus via the map $\theta \mapsto \mathcal{T}(\theta, \omega)$. There are a few theorems in use now that are titled the *KAM theorem*, and they differ mainly whether they discuss analytic or smooth perturbations. It is easier to find sources discussing the analytic versions, since they provide stronger results about the invariant tori. Having said this, we use the C^r version because it is easier to construct smooth approximations of discontinuous functions as opposed to analytic. We bring smooth approximations into the mix, since (1) alone is clearly discontinuous.

2.3 Approximating locally L^1 functions

The Hamiltonian (1) we wish to study is discontinuous, which by itself makes it not suitable for the KAM theorem. We can, however, smoothly approximate the Hamiltonian by using *mollifiers*. The KAM theorem then can be applied to the smoothed Hamiltonian, which of course means we are not directly studying (1) but instead gaining an intuition for the true behavior.

The *standard mollifier* $\varphi : \mathbb{R}^n \to \mathbb{R}$ is the following function:

$$\varphi(x) = \begin{cases} c \exp\left(\frac{1}{|x|^2-1}\right), & |x| < 1 \\ 0, & |x| \geq 1, \end{cases}$$

where $c > 0$ is a scaling factor chosen so that the integral of φ over $\mathbb{R}^n$ is 1. Also, φ is commonly called a *bump* function, since its support is compact, and its graph resembles a bump in space. For $\varepsilon > 0$, let

$$\varphi_\varepsilon(x) = \frac{1}{\varepsilon^n} \varphi\left(\frac{x}{\varepsilon}\right),$$

this function has the following properties:

$$\varphi_\varepsilon \in C_c^\infty(\mathbb{R}^n), \quad \varphi \geq 0,$$
$$\int_{\mathbb{R}^n} \varphi_\varepsilon = 1, \quad \operatorname{supp}(\varphi_\varepsilon) \subset B_\varepsilon(0) = \{x \in \mathbb{R}^n : |x| < \varepsilon\},$$

that is, the function φ_ε is smooth in $\mathbb{R}^n$ with compact support, it is positive, its integral is 1, and the support of φ_ε is fully contained in the unit ball of radius $\varepsilon > 0$ centered at the origin.

We say the function f is in the space of locally p-integrable functions $L^p_{\text{loc}}(X)$, if $f : X \to \mathbb{R}$ is measurable, and for every open $V \subseteq X$ which is compactly supported in X, the restriction of f to V satisfies $f|_V \in L^p(V)$.

Let $f \in L^1_{\text{loc}}(X)$ be a locally integrable function in $X \subseteq \mathbb{R}^n$. The *mollification* of f is defined as the convolution of f with φ_ε, that is, $\varphi_\varepsilon * f : X_\varepsilon \to \mathbb{R}$ where $X_\varepsilon = \{x \in X : d(x, \partial X) > \varepsilon\}$. Explicitly,

$$\begin{aligned} f_\varepsilon(x) = \big(\varphi_\varepsilon * f\big)(x) &= \int_X \varphi_\varepsilon(x-y) f(y) dy \\ &= \int_{B_\varepsilon(0)} \varphi_\varepsilon(y) f(x-y) dy, \quad x \in X_\varepsilon \end{aligned}$$

Some properties that the mollification f_ε has are summarized here:

Theorem 2. Let $f \in L^1_{\text{loc}}(X)$. Then the mollification f_ε has the following properties:

1. $f_\varepsilon \in C^\infty(X_\varepsilon)$,
2. $f_\varepsilon \to f$ almost everywhere as $\varepsilon \to 0$,
3. if f is continuous on X, then $f_\varepsilon \to f$ as $\varepsilon \to 0$ uniformly on compact subsebts of X,
4. if $1 \leq p < \infty$ and $f \in L^p_{\text{loc}}(X)$, then $f_\varepsilon \to f$ as $\varepsilon \to 0$ in $L^p_{\text{loc}}(X)$

Proof. The proof of this theorem can be found in Appendix C of [Eva98] ■

Theorem 2 states that we can construct a family of smooth approximations to any function f that converge to f almost everywhere.

2.4 Poincaré sections and stability of maps

The Poincaré section (and map) method is a common way of studying a continuous time dynamical system. An account of the method can be found in [Ras90] and [HSD13], we will use both sources since they are complimentary.

First recall that for a dynamical system defined by a system of differential equations $\dot{X} = F(X)$ where $F : \mathbb{R}^n \to \mathbb{R}^n$, the *flow* of the system is the collection of trajectories resulting from an open neighborhood of initial conditions. The flow is typically denoted as a map $\phi(t, x_0)$ where x_0 refers to the initial conditions, and the map $t \mapsto \phi(t, x_0)$ is a solution of the system with initial conditions x_0.

For an n-dimensional system, a *Poincaré section* is a subspace Σ of the phase-space of dimension $k < n$ such that the flow $\phi(t, x_0)$ of the system is

transverse to Σ, and for each $x_0 \in \Sigma$ there exists a time $t' > 0$ such that $\phi(t', x_0) \in \Sigma$. To be transverse means that the flow is never parallel to Σ. The second condition means that any point in U must return to Σ under the action of the flow in finite time

The *Poincaré map* or *return map* is $P : \Sigma \to \Sigma$ with $P(x) = \phi(\tau_x, x)$ where $\tau_x > 0$ is the first time the trajectory with initial condition $x \in \Sigma$ returns to Σ after leaving it. Given the map $P : \Sigma \to \Sigma$, we can consider a new discrete dynamical system with state-space Σ and governed by iterations of P. An *orbit* of a point $x \in \Sigma$ is the sequence $x_n = P^n(x)$ where $P^n = P \circ \cdots \circ P$ denotes n-fold composition of P.

We recall now two concepts: the Jacobian matrix, and stability of a periodic trajectory. Let $F : \mathbb{R}^n \to \mathbb{R}^m$ with $F = (F_1, \ldots, F_m)$ be a differentiable map, the Jacobian matrix $J_F(X)$ of the function F at the point X is an $m \times n$ matrix of partial derivatives of F of the form

$$J_F(X) = \frac{\partial(F_1, \ldots, F_m)}{\partial(x_1, \ldots x_n)} = \begin{bmatrix} \frac{\partial F_1}{\partial x_1} & \frac{\partial F_1}{\partial x_2} & \cdots & \frac{\partial F_1}{\partial x_n} \\ \frac{\partial F_2}{\partial x_1} & \frac{\partial F_2}{\partial x_2} & \cdots & \frac{\partial F_2}{\partial x_n} \\ \vdots & \vdots & \ddots & \vdots \\ \frac{\partial F_m}{\partial x_1} & \frac{\partial F_m}{\partial x_2} & \cdots & \frac{\partial F_m}{\partial x_n} \end{bmatrix} = \left[\frac{\partial F_i}{\partial x_j}\right],$$

where i and j index rows and columns, respectively. One important property of the Jacobian we will use is that it obeys the chain rule for compositions of functions. Let $F : \mathbb{R}^n \to \mathbb{R}^m$ and $G : \mathbb{R}^p \to \mathbb{R}^n$, then we have:

$$J_{F \circ G}(X) = J_F(G(X)) \cdot J_G(X),$$

where we emphasize matrix multiplication with "$\cdot$".

Let $r(t)$ with $r(0) = X_0$ be a periodic trajectory of the system $\dot{X} = F(X)$. The trajectory $r(t)$ is *stable* if for all $\varepsilon > 0$ there exists a $\delta > 0$ such that every trajectory $f(t)$ we have that:

$$\|f(0) - r(0)\| < \delta \implies \|f(t) - r(t)\| < \varepsilon, \quad \text{for all } t \geq 0.$$

In other words, a periodic trajectory is stable, if there is a neighborhood of X_0 that does not expand beyond a certain radius under the flow of the system $\dot{X} = F(X)$. A periodic trajectory that is not stable is called *unstable*.

We now state a proposition relating the eigenvalues of a Poincaré map to the stability of a periodic trajectory of a system.

Proposition 1. Let $\dot{X} = F(X)$ be a system in $\mathbb{R}^n$, suppose that $X_0 \in \mathbb{R}^n$ lies on a periodic trajectory $r(t)$. Let P be a Poincaré map defined in an open set U containing X_0. Let $\lambda_i \in \mathbb{C}$ for $1 \leq i \leq n$ be the eigenvalues of the Jacobian matrix $J_P(X_0)$, then we have the following:

1. If for all $1 \leq i \leq n$ we have $|\lambda_i| < 1$, then the trajectory $r(t)$ is stable.
2. If there exists at least one $1 \leq i \leq n$ such that $|\lambda_i| > 1$, then the trajectory $r(t)$ is unstable.

In the last case when there is an eigenvalue $|\lambda_i| = 1$, then checking the Jacobian is not enough to decide the stability of the trajectory, and more information

is needed. There is a further classification of the stability of equilibrium points of a system, that is, points X^* such that $F(X^*) = 0$ but we do not need it here.

Now, we focus on our system (1). We prove the existence of a Poincaré section, and construct it explicitly. We also explain some details of the symbolic algebra computations we performed in the Jupyter notebook in [Sil23].

Recall, that the phase-space of (1) is $\mathbb{T}^2 \times \mathbb{R}^2$, we claim that the subspaces

$$S_{\text{in}} = \left\{(x, v) \in \partial S \times \mathbb{R}^2 : v \cdot (x - 1/2) < 0\right\}, \tag{3}$$

$$S_{\text{out}} = \left\{(x, v) \in \partial S \times \mathbb{R}^2 : v \cdot (x - 1/2) > 0\right\}, \tag{4}$$

are Poincaré sections if we restrict to initial conditions on them. This greatly reduces the dynamics, and can be later used to visualize trajectories

To prove that S_{out} and S_{in} are the Poincaré sections, we will use well known results about rotations on the torus. Parametrize the torus $\mathbb{T}^2$ with angles $\theta, \varphi \in [0, 1]$, a particle in free motion on $\mathbb{T}^2$ follows the trajectory $r(t) = x_0 + vt$ where $x_0 \in \mathbb{T}^2$ is the initial condition and $v \in \mathbb{R}^2$ is the velocity. If the angle of v with respect to the axis θ is rational, then $r(t)$ is periodic, otherwise $r(t)$ is dense in $\mathbb{T}^2$.

Lemma 1. The flow of (1) induces a well-defined map $P_{\text{oi}} : S_{\text{out}} \to S_{\text{in}}$.

Proof. Let $(x, v) \in S_{\text{out}}$, at this point the solution of (1) continues with free motion $r(t) = x + vt$. If the angle of v is rational, then there exists some time t_2 at which $r(t_2) = x$, and $(r(t_2), v) \in S_{\text{out}}$. Since at time t_2 the trajectory intersects ∂S transversally, there must exist $t_1 < t_2$ such that $(r(t_1), v) \in S_{\text{in}}$. Since the trajectory intersects S_{in} at least once, there must exist a unique $t_0 \leq t_1$ such that $(r(t_0), v) \in S_{\text{in}}$.

If instead the angle of v is irrational, consider an open neighborhood $U \subseteq \partial S$ of x such that $U \times \{v\} \subseteq S_{\text{out}}$. This can be done by taking a sufficiently small interval in ∂S around x. Since $r(t)$ is dense in $\mathbb{T}$, there exists a time t_1 such that $r(t_1) \in U$. By the same reasoning as in the previous case, there exists a unique minimal time t_0 such that $(r(t_0), v) \in S_{\text{in}}$.

Define $P_{\text{oi}}(x, v) = (r(t_0), v)$, which is well-defined. ■

Lemma 2. The flow of (1) induces a well-defined map $P_{\text{io}} : S_{\text{in}} \to S_{\text{out}}$.

Proof. Let $(x, v) \in S_{\text{in}}$, under the flow of (1) the trajectory $r(t)$ follows some Larmor circle C. We know $x \in C \cap \partial S$, so since (x, v) is transversal to ∂S, there must exist a point $x_1 \in C \cap \partial S$ with $x_1 \neq x$. Hence, also there must exist a time t_0 at which the trajectory intersects S_{out}. Define $P_{\text{io}}(x, v) = (r(t_0), r'(t_0))$. ■

Now, we state the existence of the Poincaré section as a proposition and prove it.

Proposition 2. Let S be the disc of radius R centered at $(1/2, 1/2) \in \mathbb{T}^2$. The sets S_{in} and S_{out} defined in (3) and (4), respectively, are Poincaré sections for the system (1).

Proof. The map $P_{\text{i}} = P_{\text{oi}} \circ P_{\text{io}}$ is a return map for S_{in}. Likewise, $P_{\text{o}} = P_{\text{io}} \circ P_{\text{oi}}$ is a return map for S_{out}. ■

In [KS17] a similar result is proved for a configuration of finitely many bumps. In that case a different method was used that did not rely on an infinite number of bumps, in ours the reasoning was simplified due to this.

We proved the existence of the Poincaré map P_{o}, now we provide an explicit form of $P_{\mathrm{o}} : S_{\mathrm{out}} \to S_{\mathrm{out}}$ that is more convenient for computations. We specifically take S_{out} and S_{in} as the circles with radius R center at $(1/2, 1/2)$ in $\mathbb{T}^2$ and with their respective orientation of the velocity vectors. We define P_{o} as the composition

$$P_{\mathrm{o}} = \psi^{-1} \circ A_2 \circ \pi \circ A_1 \circ \psi,$$

where $\psi : S_{\mathrm{out}} \to \psi(S_{\mathrm{out}})$ takes polar coordinates to Cartesian,

$$\psi(\theta, \varphi) = \left(R\cos\theta + \frac{1}{2}, R\sin\theta + \frac{1}{2}, \cos\varphi, \sin\varphi \right),$$

$A_1 : \psi(S_{\mathrm{out}}) \to \mathbb{R}^2 \times \mathbb{R}^2$ finds the first positive time intersection of a ray $(x + vt, y + wt)$ with the lattice of circles of radius R and centered at $\mathbb{Z}^2 + 1/2$,

$$A_1(x, y, v, w) = (x + vT, y + wT, v, w),$$
$$\text{with } T = \min_{n,m\in\mathbb{Z}} \left\{ t > 0 : \left\| \left(x + vt - n - \frac{1}{2}, y + wt - m - \frac{1}{2} \right) \right\| = R \right\},$$

the value of T can be determined explicitly by solving for the roots of a quadratic equation. In practice, one would like to know the pair n, m that minimizes the expression ahead of time, for example, when the map is computed for a known periodic trajectory. Next, $\pi : \mathbb{R}^2 \times \mathbb{R}^2 \to \mathbb{T}^2 \times \mathbb{R}^2$, is the typical quotient map taking the plane to the 2-torus,

$$\pi(x, y, v, w) = (\lfloor x \rfloor, \lfloor y \rfloor, v, w).$$

Next, $A_2 : \psi(S_{\mathrm{in}}) \to \psi(S_{\mathrm{out}})$ encompasses the influence of the magnetic field, for $X = (x, y, v, w)$ we have

$$A_2(X) = \frac{1}{\alpha^2 + \beta^2} \begin{bmatrix} \alpha^2 - \beta^2 & 2\alpha\beta & 0 & 0 \\ 2\alpha\beta & \beta^2 - \alpha^2 & 0 & 0 \\ 0 & 0 & \beta^2 - \alpha^2 & -2\alpha\beta \\ 0 & 0 & -2\alpha\beta & \alpha^2 - \beta^2 \end{bmatrix} \begin{bmatrix} x - \frac{1}{2} \\ y - \frac{1}{2} \\ v \\ w \end{bmatrix} + \begin{bmatrix} \frac{1}{2} \\ \frac{1}{2} \\ 0 \\ 0 \end{bmatrix}$$

where $(\alpha, \beta) = (x + v/b - 1/2, y - w/b - 1/2)$ is the center of the Larmor circle of the trajectory with initial position (x, y) and velocity (v, w) but is shifted by $(-1/2, -1/2)$ for reasons we explain now.

The function A_2 can be constructed using some plane geometry and linear algebra. Consider two circles C_1, C_2 in the plane with centers a_1, a_2, respectively. Let A denote the reflection in the line ℓ containing a_1 and a_2. We notice that C_1 and C_2 are invariant under the action of A and are symmetric with respect to the reflection, so if C_1, C_2 intersect in two points, and we know one point z, we know the other is Az. Suppose now v is a tangent vector of C_1 at z, then Av is a tangent vector at Az. Lastly, we take $-Av$, since we need it to point in the opposite direction, that is, if v points into C_2, then $-Av$ points outwards.

Coming back to the definition of A_2, the matrix represents a reflection in the line parallel to ℓ and passing through the origin. The translations $\pm(1/2, 1/2, 0, 0)$ are needed to account for the fact the matrix reflects in the wrong line. We can construct the matrix via its diagonalization, by picking appropriate eigenvalue, eigenvector pairs. We pick $v_1 = (\alpha, \beta)$ with 1, since it is parallel to ℓ, and we pick $v_2 = (-\beta, \alpha)$ with -1, since it is orthogonal to ℓ. Let $D = \text{diag}(-1, 1)$ be a diagonal matrix with $-1, 1$ on the diagonal, and let $M = [v1\ v2]$, then MDM^{-1} gives the matrix.

Finally, the map $\psi^{-1} : \psi(S_{\text{out}}) \to S_{\text{out}}$ switches back to polar coordinates and is given by

$$\psi(x, y, v, w) = \left(\text{arctan2}\left(y - \frac{1}{2}, x - \frac{1}{2}\right), \text{arctan2}(w, v)\right).$$

This form for P_{o} seemed to be the simplest and most convenient we could find for symbolic algebra. For numerical computations, some changes had to be made for the sake of efficiency, though we will not discuss this here.

The map P_{o} contains many moving parts due to the composition of 5 maps. We cannot provide the Jacobian J_P explicitly, since the expression would take up many pages and not add anything to the discussion. The situation gets worse when we try to analyze the stability of fixed points of P_{o}^n for $n > 1$, for example we will do so for $n = 2, 4$, ane 8. Still, it's nice to mention some ways to simplify the computations. By the chain rule,

$$J_{P_{\text{o}}} = J_{\psi^{-1}} J_{A_2} J_\pi J_{A_1} J_\psi,$$

where we suppressed the arguments for the Jacobians in the notation. We notice that $J_\pi = I$ for points in the interior of squares $[n, n+1] \times [m, m+1]$ for $n, m \in \mathbb{Z}$, since for such points π is locally a translation. Then, composing $J_{P_{\text{o}}}$ we see

$$J_{P_{\text{o}}}^n = \left(J_{\psi^{-1}} J_{A_2} J_\pi J_{A_1} J_\psi\right)^n = J_{\psi^{-1}} \left(J_{A_2} J_{A_1}\right)^n J_\psi,$$

so, we only need to convert between polar and Cartesian at the beginning and end. Likewise, we can show that the coordinate conversions cancel out when composing P_{o}. The above form of P_{o} and $J_{P_{\text{o}}}$ were used in [Sil23], in a later section we will provide some examples of our results.

2.5 Symbolic dynamics and semi-conjugacy

In this section we recall the basics of symbolic dynamics and topological semi-conjugacy of dynamical systems, we follow the relevant sections in [HSD13].

For $N \in \mathbb{N}$ consider the *shift space* $\Sigma_N = \{0, 1, \dots, N-1\}^{\mathbb{N}}$, the space of sequences consisting of N symbols. We can endow Σ_N with a metric:

$$d(x, y) = \sum_{n \in \mathbb{N}} \frac{|x_n - y_n|}{N^n}.$$

With this metric Σ_N is also a compact metric space. On Σ_N we can consider the shift map:

$$\sigma : \Sigma_N \to \Sigma_N$$
$$(x_1, x_2, x_3, \dots) \mapsto (x_2, x_3, \dots),$$

that is, we shift the indices to the left, and drop the first element. The map σ is uniformly continuous. Together with σ, the space Σ_N becomes a discrete dynamical system. It can be proven directly with straight-forward techniques that this system is, in fact, chaotic by Devaney's definition: the system is transitive, and the set of periodic orbits is dense.

Proving directly that a system is chaotic in general is difficult, so another method should be used. This is where *(semi)-conjugacies* come in. Two maps $f : I \to I$ and $g : J \to J$ on topological spaces I and J are *conjugate* if there exists a homeomorphism $h : I \to J$ such that $h \circ f = g \circ h$. Likewise, f and g are *semi-conjugate* if there exists a continuous surjective map $h : I \to J$ satisfying the same equation. One important result about (semi)-conjugacies is the following:

Proposition 3. Suppose $f : I \to I$ and $g : J \to J$ are (semi)-conjugate via $h : I \to J$, where both I and J are compact metric spaces. If f is chaotic on I, then g is chaotic on J.

Another simple result is that a conjugacy preserves periodic orbits and their period, that is since $h \circ f = g \circ h$ implies $h \circ f^n = g^n \circ h$, where f^n means we compose f a total of n times. For semi-conjugacies we have a similar result, periodic orbits are mapped to periodic orbits however their periods need not be preserved. Hence, we can discern a lot about a system if we construct a (semi)-conjugacy to, for example, Σ_N. This is the core of symbolic dynamics.

2.6 The Lempel-Ziv compression algorithm

Here we introduce the Lempel-Ziv complexity (LZC) as described in [LZ76], give some basic examples, and describe some cases where it was used effectively. We suggest as reading the original paper [LZ76], the article [KS87] for nice examples, and [Ras90] for a easily digestable summary of LZC.

LZC operates on finite length sequences, *strings*, of symbols by applying a compression algorithm, the complexity of the original sequence is then quantified by the result of the compression. For convenience, for a string $A = a_1 a_2 \dots a_n$ we define the notation $A(i, j) = a_i \dots a_j$ to denote a *substring*. Below we give the LZC algorithm.

```
1 Input a string A of length n;
2 Define the number of words C = 1;
3 Define i = 2;
4 Repeat forever:
5   Determine the longest k for which there exists an index j < i
      such that A(j,j+k) is the same as A(i,i+k);
6   Increment i by k+2;
7   Increment C by 1;
8   If i >= n go to line 9, otherwise return to line 4;
9 Output C;
```

We provide examples below. The $\cdot$ is used as a substring delimiter, the overline indicates the longest substring $A(i, i + k)$ that was found and the underline indicates where we found it, i.e., $A(j, j + k)$. Notice the starting index of the

longest substring is not necessarily unique.

$$\begin{aligned}
01011010001101110010 &\xrightarrow{(1)} \underline{0}\cdot\overline{1}01101000110111 0010\\
&\xrightarrow{(2)} \underline{0\cdot 1\cdot \overline{01}}\overline{10}10001101110010\\
&\xrightarrow{(3)} \underline{0\cdot 1\cdot 011}\cdot\overline{0100}01101110010\\
&\xrightarrow{(4)} 0\cdot 1\cdot \underline{011\cdot 010}0\cdot\overline{01101\overline{1}}10010\\
&\xrightarrow{(5)} 0\cdot 1\cdot 011\cdot 0\underline{100\cdot 0}11011\cdot\overline{1001\overline{0}}\\
&\xrightarrow{(6)} \underline{0\cdot 1}\cdot 011\cdot 0100\cdot 011011\cdot 1001\cdot\overline{0}\,,
\end{aligned}$$

the number of substrings is 7, so the LZC of this sequence is 7. Let's consider another example with repetition:

$$\begin{aligned}
01101101101101101101 &\xrightarrow{(1)} \underline{0}\cdot\overline{1}101101101101101101\\
&\xrightarrow{(2)} 0\cdot\underline{1\cdot\overline{10}}1101101101101101\\
&\xrightarrow{(3)} 0\cdot\underline{1\cdot 10\cdot\overline{1101101101101101}}\,,
\end{aligned}$$

the number of substrings is 4, so the LZC is 4. Notice how the two examples have the same number of digits but the one with less repetition has greater complexity. We consider one final example:

$$\begin{aligned}
0101010101010101010101 &\xrightarrow{(1)} \underline{0}\cdot\overline{1}0101010101010101010101\\
&\xrightarrow{(2)} \underline{0\cdot 1\cdot\overline{0101010101010101}01}\,,
\end{aligned}$$

and we see the LZ complexity is 3. Notice that even though the last two examples are periodic, one has greater LZC, since the repeating substring 011 is longer than 01. So, LZC not only differentiates between periodic and aperiodic sequences, it also distinguishes between periodic sequences of different period.

All examples were with the alphabet $\{0,1\}$ but this can be done with an arbitrary alphabet. It's interesting to note that the LZC algorithm supports infinite alphabets. The alphabet is taken to be finite because then one can compute a lower theoretical bound on the LZC for the chosen alphabet, and meaningfully compare the complexity of sequences: a sequence with LZC close to the bound is likely to be random, while if the LZC is low comparative to the bound, then the sequence may be (quasi)-periodic.

In [KS87] the authors used LZC to analyze a time series resulting from the logistic map, and a system of coupled logistic maps. They determined that LZC can be used to discern whether a signal is random or approaching an equilibrium or a periodic trajectory. They noticed that despite its strength in detecting structures like attractors, the LZC does not however give information about the structure itself.

3 Weak magnetic fields and KAM theory

In this section we will study the dynamics of (1) for "small" values of b, and use the KAM theorem to motivate our ideas. We claim that (1) can be viewed as a perturbation of at least two different Hamiltonian systems. In one case, we can consider (1) as a perturbation of $H^0(q,p) = \|p\|^2/2$ on $\mathbb{T}^2$, that is, free motion on the 2-torus. In the other case, we can consider it as a perturbation of a uniform magnetic field in $\mathbb{R}^2$. We corroborate our reasoning with numerical simulations which can be found in the notebook `Figures.ipynb` at [Sil23].

One thing to notice immediately is that the magnetic potential A is discontinuous along ∂S, what we will see is that the perturbation term H^1 in $H = H^0 + bH^1$ is also discontinuous due to this, so we cannot directly apply the KAM theorem to H. To address this we introduce mollifiers to smoothly approximate H^1 by $\hat{H}^1 = \varphi_\varepsilon * H^1$, we can then apply the KAM theorem to $\tilde{H} = H^0 + b\hat{H}^1$. Of course, using such an approach, we do not make statements about H, instead we do so for $\tilde{H}$. We insist however that we can still motivate a lot about the behavior of H by the theory that applies to $\tilde{H}$.

3.1 Investigating small magnetic field strengths

In fig. 2 we numerically solve system (1) and observe some interesting relations. Each plot shows 5 trajectories varying $b = 10^{-1}, \ldots, 10^{-5}$. In fig. 2a and 2b the initial conditions and parameters are the same $X \approx (0.38, 0.81)$ and $V \approx (0, 1)$, and $R = 1/3$, only the duration of the simulation is longer in fig. 2b. In fig. 2c, V is the same, $X \approx (0.44, 0.65)$ and $R = 1/6$.

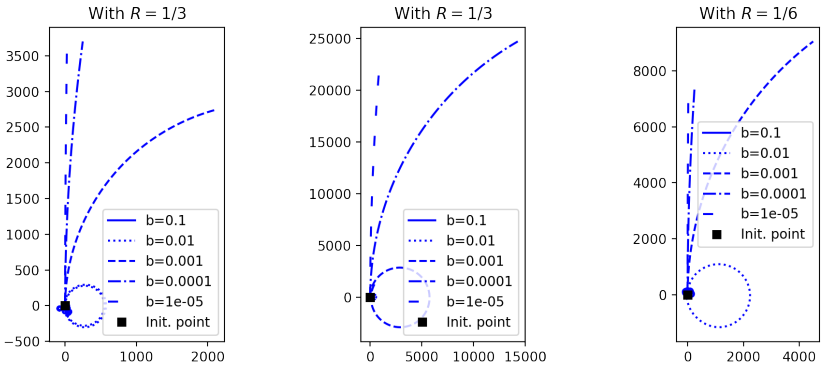

(a) (b) (c)

Figure 2: For the smallest b, the trajectories resemble straight lines for a long time. As b increases, the trajectories appear to bend more and form circular paths. This motivates viewing the system as a perturbation of either free motion in $\mathbb{T}^2$ or of motion in a uniform magnetic field in the plane.

First, we see in each figure that the trajectory for $b = 0.1$ appears as a smear near the origin, this is likely because b is large enough for the deflection in each disc to no longer be considered a small perturbation. We note, however, in later sections we also find circle-like quasiperiodic trajectories for significantly larger values of b. The difference here is that the circular arcs here seem to be

generic, while for larger b the circle-like trajectories are more scarce and each has a smaller region of stability.

For the values of $b < 0.1$ we can make two observations. First, for very low b, the trajectories start out rather straight and only accumulate a deflection after a long time. This is the behavior we see in $\mathbb{R}^2$, in $\mathbb{T}^2$ we expect rotations with some drift. For particular choices of b and intial conditions, we could expect that after a number of rotations in $\mathbb{T}^2$, the drift adds up in a way that makes the trajectory closed. This motion motivates perturbing free motion on $\mathbb{T}^2$.

The other observation is that for sufficiently long times, it looks like the trajectories form circles in $\mathbb{R}^2$. This motivates the idea to perturb a uniform magnetic field in the plane.

3.2 Perturbations of linear motion

Here we will use the KAM theorem to motivate the idea of viewing the motion we find in fig. 2 as a perturbation of free motion on $\mathbb{T}^2$. First, let us determine a Hamiltonian H^1 such that $H = H^0 + bH^1$ and $H^0 = \|p\|^2/2$. Denoting $A = (A_1, 0)$, we see:

$$\begin{aligned} H(q,p) = \frac{1}{2}\left\|p - A(q)\right\|^2 &= \frac{1}{2}\left(p_1 + A_1(q)\right)^2 + \frac{1}{2}p_2^2 \\ &= \frac{\|p\|^2}{2} + \frac{1}{2}\left(2p_1A_1(q) + A_1^2(q)\right) \\ &\overset{(\star)}{=} H^0(p) + bH^1(q,p,b), \end{aligned}$$

where in $(\star)$ we used that we can factor out b from $A_1(q)$. As previously discussed, H^1 is discontinuous, so to apply KAM, we need to mollify H^1. Hence, consider the mollified perturbation $\hat{H}^1 = \varphi_\varepsilon * H^1$, where $\varepsilon > 0$ is independent of b. We see H^0 is real analytic, it is also in action-angle coordinates, since we consider the motion on $\mathbb{T}^2$. We also see H^0 is non-degenerate: $\det \partial_p^2 H^0 = 1 \neq 0$, and the frequency map $\partial_p H^0(p) = p$ is a diffeomorphism. Now, by theorem 1, for sufficiently small $b_* > 0$ there are tori of H^0 that are preserved under the perturbation $\hat{H}^1$.

Since $\hat{H}^1$ is always smooth, the above reasoning is valid for any $\varepsilon > 0$. The caveat is that the KAM theorem may provide for each choice of ε a different $b_* := b_*(\varepsilon)$, i.e., it is a function of ε. The question that we should answer then is whether $b_* \to 0$ as $\varepsilon \to 0$, that is whether the reasoning is valid and useful in the limit. We determined that this is difficult, and did not pursue the answer.

3.3 Perturbation of motion in a constant field

In this section we first motivate why we can consider the motion of (1) as perturbed motion of a uniform magnetic field in the plane, and afterwards provide some numerical evidence supporting the claim.

We first reason heuristically to see that the idea is valid. Comparing the trajectories for $b = 0.01$ and 0.001 in fig. 2a and 2b, we see that the radius of the trajectory is ≈ 250 and ≈ 2500, respectively. If we assume this is the value of the Larmor radius $\hat{L}$ in each case, then we see $\hat{L} \propto 1/b$ or $\hat{b} \propto b$. Now, comparing the trajectories for $b = 0.01$ in fig. 2a and 2c, we see halving the radius R of the magnetic bumps roughly quadruples the radius $\hat{L}$ from 250 to

1000, that is, $\hat{L} \propto 1/R^2$, and the strength then relates as $\hat{b} \propto R^2 b$. The task then is to determine $C \in \mathbb{R}$ such that $\hat{b} = CR^2 b$.

We can reason more directly by comparing fluxes. Focusing on $U = [0,1]^2$, we would like the unperturbed uniform field $\hat{B} = (0, 0, \hat{b})$ to deflect trajectories on U as would the piecewise defined B of (1). How much a trajectory is deflected depends on the flux of the field, since the flux measures the "flow" of the field through a surface. Equating the fluxes $\Phi_B(U) = \Phi_{\hat{B}}(U)$, we can compute the required strength $\hat{b}$ for $\hat{B}$. In our case, this implies $\hat{b} = \pi R^2 b$, which is about what we expected.

Now, we should numerically test this hypothesis. To test the validity of the relation, we give two tests, the results of which can be found in fig. 3.

The first test:

1. For $1 \leq i \leq 50$, sample (R_i, b_i) uniformly from $[0.25, 0.45] \times [10^{-10}, 10^{-6}]$
2. For R_i, b_i uniformly sample initial conditions X_{ij}, V_{ij} with $1 \leq j \leq 20$.
3. Using the method in [Coo93], fit a circle to the trajectory of each X_{ij}, V_{ij}, the radius of which is $\hat{L}_{ij}$. We take the average $\hat{L}_i = \sum_{j=1}^{20} \hat{L}_{ij}/20$.
4. Via a least squares method, we fit a general cubic:

$$a_0 + a_1 R_i + a_2 b_i + a_3 R_i^2 + a_4 R_i b_i + a_5 b_i^2 + a_6 R_i^3 + a_7 R_i^2 b_i + a_8 R_i b_i^2 + a_9 b_i^3 = 1/\hat{L}_i.$$

The second test is similar, we fix $R_i = 1/3$, and fit a line $a_0 + a_1 R_i^2 b_i = 1/\hat{L}_i$. We opt to fit a general cubic function to avoid any bias in reasoning. We should expect after fitting that only a_7 contributes significantly.

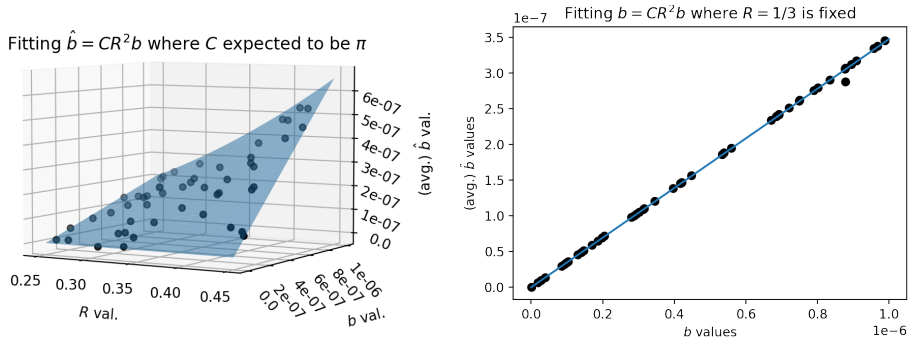

(a) Fitting a cubic surface

(b) Fitting a line

Figure 3: We conjectured that the motion of (1) for a range of b is comparable to the motion of a uniform magnetic field in the plane with field strength $\hat{b} = CR^2 b$ for some $C \in \mathbb{R}$. We collected data and fit a cubic and a line, in each case we find $C = 3.2$ and $C = 3.12$, respectively, which is $\approx \pi$.

The coefficients of the fitted cubic surface in fig. 3a come out as

$$
\begin{aligned}
&a_0 \approx 6.7 \cdot 10^{-8}, && a_1 \approx -6.2 \cdot 10^{-7}, && a_2 \approx 6.7 \cdot 10^{-3},\\
&a_3 \approx 1.9 \cdot 10^{-6}, && a_4 \approx -5.3 \cdot 10^{-2}, && a_5 \approx -1.9 \cdot 10^{+2},\\
&a_6 \approx -1.8 \cdot 10^{-6}, && a_7 \approx 3.2, && a_8 \approx -6.6 \cdot 10^{+1},\\
&a_9 \approx -3.0 \cdot 10^{-4}, &&&&
\end{aligned}
$$

The values of a_0 to a_4, a_6 and a_9 are negligible as expected, likewise $a_7 \approx \pi$. We notice that a_5 and a_8 are quite large but we reason that the contribution of their respective monomial term is still small, since both contain a factor of b^2 which has an order of magnitude at most 10^{-6}. The coefficients of the fitted line in fig. 3b are $a_0 \approx 4.4 \cdot 10^{-10}$ and $a_1 \approx 3.12$, which can be explained in the same way. So, the relation $\hat{b} = \pi R^2 b$ seems valid, and this motivates perturbing a uniform magnetic field into the bump field.

Overall, the results show that our assumptions are plausible, we approximately see π in the coefficient. The results are not as precise as desired but that can be due to randomly choosing the initial conditions for the trajectories. The circular trajectories correspond to invariant tori, and since not all tori are preserved under the perturbation, we expect that, chosen at random, some trajectories will not follow closely a circular path. Similarly, the chosen range for sampling R and b could be too large, though in tests we made that we omit here, we noticed that the relation holds more or less for a wider range of $[0.1, 0.45] \times [10^{-16}, 10^{-2}]$.

We conclude this section by stating a conjecture motivated by the numerical findings demonstrated above.

Conjecture 1. There exists an open subset $V \subset (0, 1/2) \times (0, \infty)$ such that for all $(R, b) \in V$ the phase-space of (1) contains an open set of initial conditions resulting in trajectories that are close, in some appropriate sense, to trajectories arising due to a uniform magnetic field $B = (0, 0, \pi R^2 b)$.

4 Complexity and symbolic dynamics

In this section we consider the dynamics of (1) for large b, that is, in the case where KAM and perturbative methods are not readily applicable. We approach the system in an exploratory way: we first consider some simple examples of periodic trajectories we found by hand, and analyze their stability. Afterwards, we search for more complicated behaviors.

The examples we find by hand range from simple to rather complicated, and both stable and unstable. The existence of these periodic trajectories of varying complexity motivates the search for more examples. Furthermore, to make the search more systematic, we introduce new numerical methods.

Using the Poincaré section we constructed in section 2.4 we will map trajectories of (1) to a shift space Σ and analyze the complexity of these trajectories with the Lempel-Ziv complexity. What we find is rich dynamics and a visual method of analysis well suited for similar problems.

4.1 First periodic trajectories and stability analysis

We begin our analysis by showing some (quasi)-periodic trajectories that we found by hand. For some of them we analyzed their stability using the Poincaré section method with the help of a computer algebra system. Throughout we reference results produced using `Sympy` that we documented in [Sil23].

For each figure below, on the left is the trajectory in the plane, and on the right is the trajectory restricted to the Poincaré section S_{out} as viewed on $\mathbb{T}^2$. The depth of computation is 2000 iterations of P_{o}, unless stated otherwise.

The trajectory in fig. 4a is periodic, by visual inspection we can determine that its minimal period is 4. To see this we can count how many times the trajectory enters S_{out} on the plot. Hence, to analyze the stability of this trajectory, we need to determine the eigenvalues of $J_{P_{\text{o}}^4}$ and apply proposition 1. We determined with the help of `Sympy` that the eigenvalues of $J_{P_{\text{o}}^4}$ at $(0,0)$ are

$$\lambda_+ = -\frac{1}{2} + \frac{\sqrt{3}}{2}i, \quad \lambda_- = -\frac{1}{2} - \frac{\sqrt{3}}{2}i,$$

where we see $|\lambda_\pm| = 1$. So, in this case, proposition 1 cannot tell us whether the system is stable or not. The eigenvalues suggest that iterates of P_{o}^4 starting near $(0,0)$ experience a rotation motion. Since, $|\lambda_\pm| = 1$, it is not clear whether the iterates at some point escape from $(0,0)$. However, in fig. 4b we see that the iterates around $(0,0)$ organise into an ellipse, further suggesting that the trajectory at $(0,0)$ is stable.

Applying the same reasoning as before to the trajectory in fig. 4c, we check the eigenvalues of $J_{P_{\text{o}}^8}$ at $(0,0)$ which are precisely

$$\lambda_\pm = -159432\sqrt{2} + \frac{1803761}{8} \pm \frac{\sqrt{21}\sqrt{309863321949 - 219106456192\sqrt{2}}}{8},$$

approximately they are $\lambda_\pm \approx -0.772 \pm 0.636i$. Again, we notice that $|\lambda_\pm| = 1$, so the Jacobian cannot inform us on the stability. Then again, fig. 4d suggests that the trajectory is stable.

Meanwhile, fig. 5a, fig. 5b seem to be unstable or have very small regions of stability, in fact, the plots are given only to 35 iterations due to sensitivity. To

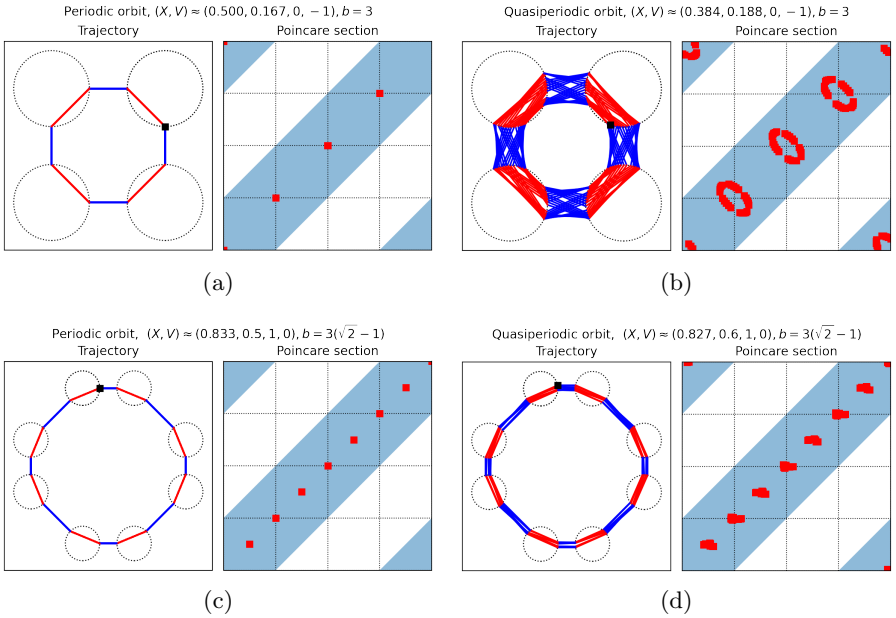

Figure 4: On the left are periodic orbits and on the right are perturbations. This suggest that the periodic orbits are stable, however the results of the Jacobian test using the Poincaré return map were inconclusive, since in both cases the eigenvalues were complex with norm 1.

study the stability of fig. 5a we considered the one parameter family of initial condtions $(\theta, \varphi) = (\delta, 0)$ for $0 < \delta < \pi/2$ and field strength $b = 3/\sin\delta$.

Notice that as $\delta \to \pi/2$, we have $b \to 3$, which would mean the Larmor circle of the trajectory would have the same radius as the magnetic disc. This limiting case does not occur but for $\delta \approx \pi/2$ we see a relatively large radius. It is not unlikely that in this limit, the trajectories are unstable, since they come so close to the boundary. If instead we consider $\delta \to 0$, we see $b \to \infty$ and as discussed before, in this limit, the system reduces to a classical periodic Lorentz gas, which supports the case for instability. We computed the eigenvalues of $J_{P_o^2}$ at $(\delta, 0)$ for this family and see

$$\lambda_\pm = \frac{\cos^2\delta - 12\cos\delta + 18}{\cos^2\delta} \pm \frac{2\sqrt{3}\sqrt{3 - 2\cos\delta}\,(\cos\delta - 3)}{\cos^2\delta}.$$

It can be determined graphically that both $\lambda_\pm \in \mathbb{R}$, furthermore $|\lambda_+| < 1$ and $|\lambda_-| > 1$, which means that we have a one parameter family of unstable trajectories. We did not conduct the same analysis for the trajectory in fig. 5b but expect the trajectories to be unstable.

We note that the trajectory in fig. 4a also belongs to a one parameter family of periodic orbits with $(\theta, \varphi) = (\delta, 0)$ and $b = 3/(\sin\delta + \cos\delta)$ for $\delta \in (-\pi/4, \pi/2)$ but we could not find an expression for the eigenvalues in this case because the computation time was unreasonably long which was probably due to the algebra system not being able to simplify the trigonometric expressions in any meaningful way. Since we have evidence that $(\theta, \varphi) = (0, 0)$ with $b = 3$ is a stable

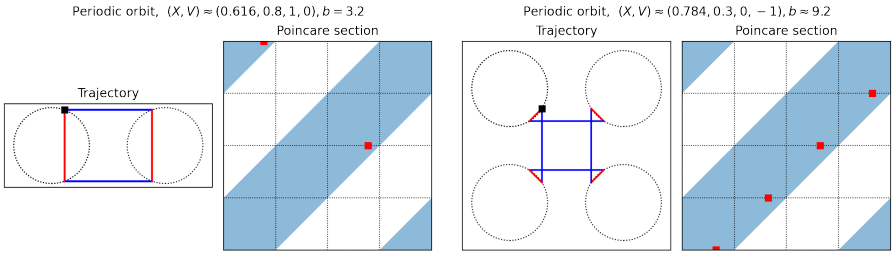

(a) (b)

Figure 5: The left periodic orbit was verified using the Jacobian test to be unstable. The right orbit is also believed to be unstable, though this has not bee proven.

trajectory, we expect there exists an interval $I = (-\varepsilon, \varepsilon) \subseteq (-\pi/4, \pi/2)$ with $\varepsilon > 0$ such that for all $\delta \in I$, the trajectory for $(\delta, 0)$ and $b = 3/(\sin\delta + \cos\delta)$ is also stable.

Having analyzed these examples, we have an idea of what kind of behavior to expect from (1). We expect both stable and unstable periodic trajectories, however to continue studying periodic trajectories we need a more systematic way of finding periodicity. We continue with this in the next sections.

4.2 Symbolic dynamics of the magnetic Sinai billiard

Recalling that the system (1) has a Poincaré section S_{out} with a Poincaré map $P : S_{\text{out}} \to S_{\text{out}}$ as proven in section 2.4, we would like to find a shift space Σ_N for $N \in \mathbb{N}$ and a (semi)-conjugacy $h : S_{\text{out}} \to \Sigma_N$ to reduce the system further and analyze the dynamics on the shift space. What we actually do is a bit different, we pick a shift space Σ with a countably infinite alphabet, and we do not check whether h is a (semi)-conjugacy. We explain our reasoning below.

Let $A = \mathbb{Z}^2$ be our alphabet, and consider the shift space $\Sigma = A^{\mathbb{N}}$. Here we take S_{out} in $\mathbb{R}^2$ instead of $\mathbb{T}^2$, that is, S_{out} is the union of the outward pointing boundaries of discs centered at $\mathbb{Z}^2 + 1/2$. So, $P : S_{\text{out}} \to S_{\text{out}}$ takes values in all of $\mathbb{R}^2$ and not just $[0, 1]^2$. Now, define the map $h : S_{\text{out}} \to \Sigma$ as:

$$\begin{aligned} h &: S_{\text{out}} \to \Sigma \\ h(x) &= \lfloor P(x) \rfloor - \lfloor x \rfloor \end{aligned}$$

where $\lfloor \cdot \rfloor$ is applied entry-wise. We see that $\lfloor x \rfloor$ and $\lfloor P(x) \rfloor$ are both a pair of integers, they are also $1/2$ off the coordinate of the disc $P(x)$ and x are on, hence h maps x to the displacement between x and $P(x)$ when clamped to the lattice $\mathbb{Z}^2 + 1/2$. As an example, recall the trajectory in fig. 1b. We give the first few symbols of this trajectory, starting from the black square:

$$(1, 0),\ (1, -1),\ (-1, -1),\ (-2, 1),\ (1, 2),\ (1, 0), \ldots,$$

and for example we see that the LZC of the first 5 strings is 5, since they are all unique.

Since A is countably infinite, the typical metric as discussed in section 2.5 cannot be used to make Σ a compact metric space. With the choice of alphabet

A, we cannot use the theory in section 2.5 to definitively prove that (1) has chaotic components.

Despite the above mentioned drawbacks, we insist this choice is sufficient. We had introduce the LZC in section 2.6, and we find later that the symbols produced by the map h are enough to distinguish between quasi-periodic behavior and seemingly "random" behavior. Note, that once we compute some finite sequence of symbols, computing the LZC of the sequence is done just as in the examples in section 2.6. Despite the fact A is countably infinite, and not finite, this is not an issue for computing the LZC, since the complexity is capped by the length of the sequence. So, even if A is infinite, we can only observe finitely many symbols in a finite string.

4.3 Lempel-Ziv varying b and initial conditions

In this section we focus on fig. 6, 7, and 8, they give us a good idea of the "landscape" of dynamics of (1). The figures present the LZC of a slice of initial conditions and parameters much like a bifurcation diagram. What we find and describe are regions of low complexity of varying size and structure.

To create fig. 6 we computed trajectories for varying initial conditions and parameter b, specifically, we computed the trajectories for:

$$\left(\frac{1}{2}+\sqrt{R^2-\left(y-\frac{1}{2}\right)^2}, y, 1, 0\right) \text{ for } y \in \frac{1}{2}+0.32\cdot[-1,1],$$
$$\text{and } b \in [0.001, 5],\ R=\frac{1}{3},$$

where we sampled y and b in 500 equidistant points, and the trajectories were computed to a depth of 128 iterations. For fig. 7 we did the same except we varied $b \in [0.1, 1]$. The color in the plots indicates the LZC of the sampled trajectory. From the colorbar on the right, we see blue indicates low LZC, red intermediate, and yellow high LZC. The colors are scaled between the lowest and highest LZC in the plot, so colors in separate plots may vary. Also, notice the colorbar is scaled logarithmically, this improves legibility.

We immediately notice large regions of uniformly low LZC scattered across the plots, these suggest regions of stable quasi-periodic behavior. This is corroborated by the fact that in fig. 6 the trajectory for $(y, b) = (1/2, 3)$, corresponding to the periodic orbit in fig. 4a, lands inside one of these low LZC regions, and far from the boundary. In fact, the initial conditions for all of the quasi-periodic orbits we discovered can be found in either of these plots.

We note the color of the regions differs, indicating that the behavior producing the regions is qualitatively different. The regions do not seem to be arranged in any specific pattern, yet they all seem to have a similar structure: that being 1, 2, or 3 "bulbs". It might be that the number of bulbs may change depending on the resolution of the plot and depth of the interations. Figure 7 also suggests quasi-periodic trajectories exist for a large range of b, also for b in the range of our KAM results.

If we repeat the same analysis for smaller b, the details are harder to discern. Focusing on $b \in (0.2, 0.4)$ in fig. 7, we still see the stable regions as before, however the color blends with the surrounding noise. This can be explained by

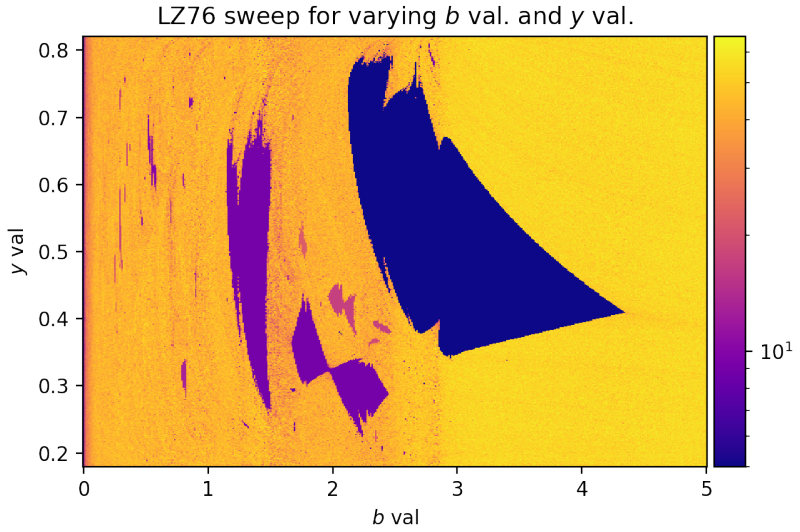

Figure 6: We take a 2-parameter family of initial conditions and visualize the Lemple-Ziv complexity (LZC). We see large regions of low complexity, suggesting that there should be periodic orbits present in these regions. The regions appear to also have varying complexity.

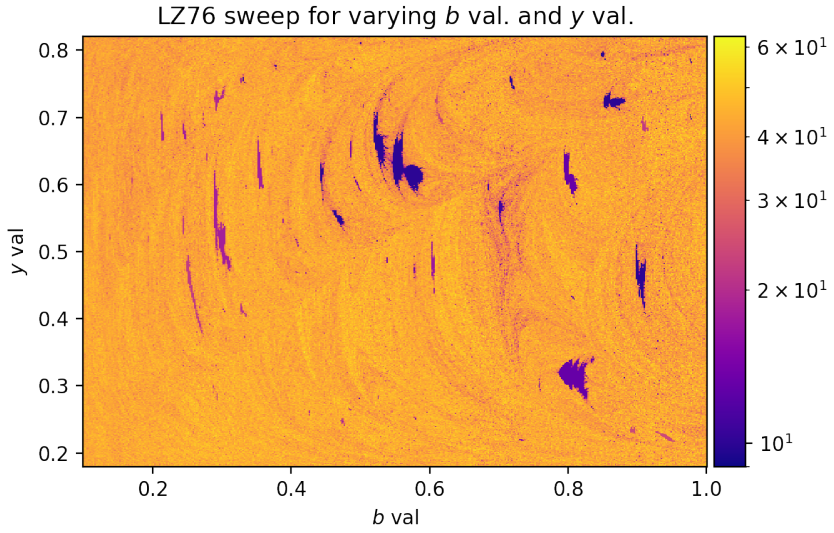

Figure 7: Here we consider the LZC for a narrower range of b and find a similar picture. There are regions with low complexity but they are smaller in size.

the effect mentioned: the period of the trajectories is comparable to the time horizon, so periodicity is less distinguishable from noise.

Lastly, we discuss the boundary of the regions. Note that for $b \in (2, 3)$ and $y \in (0.7, 0.8)$ the plot seems grainy, in fact, zooming in, we find fractal-like behavior which can be seen in fig. 8. This is in contrast to the rest of the

boundary which seems differentiable. We do not provide a figure but zooming in on the boundary for $b \in (3, 4)$ we see it is also grainy. It is not clear whether the noise is due to intrinsic structure or precision error.

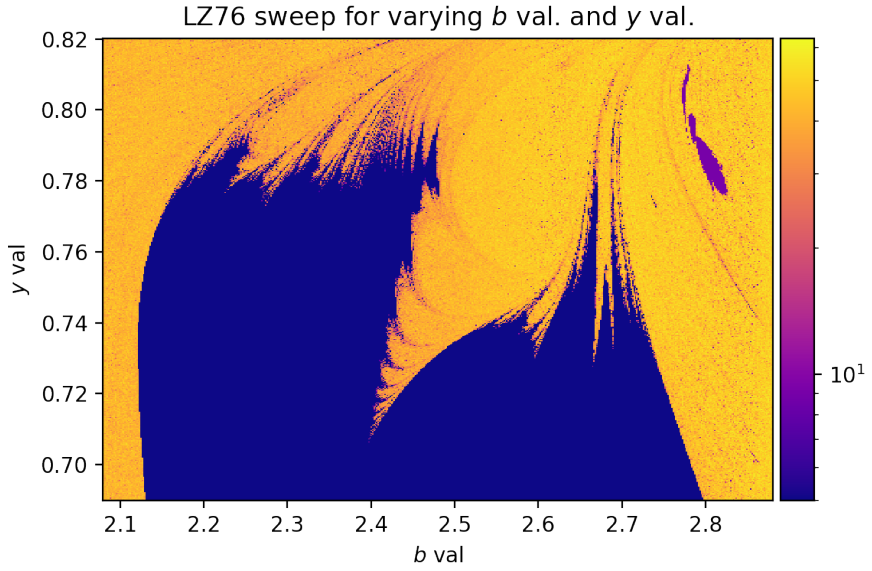

Figure 8: Zooming in on another region we find fractal like structures. At this scale it seems that these structures are localized in some parts on the boundary of the low complexity regions instead of present along the whole boundary.

Apart from regions of stability, there is a sea of high and noisy LZC throughout the plots. Closer inspection shows specks with low LZC, it is not clear whether these specks are trajectories like fig. 1b or if they correspond to quasi-periodic regions with a very small radius of stability. Focusing on fig. 6, there is a peculiar vertical line at $b \approx 2.8$. On the right of this line the average LZC looks higher than to the left, we are curious whether there is any significance to this or if it is just a coincidence. Lastly, we also checked the plot for $b \in (5, 10)$ and found the same behavior as $b \in (4.3, 5)$: high LZC with no stable regions.

Using symbolic dynamics together with LZC we have probed a rich landscape of behavior. The choice of initial conditions and parameters for the above figures was deliberate, so it is interesting to ask whether we can expect a similar landscape for other choices. For example, will the view change if we vary velocity at a point, or if we pick a different radius $R \neq 1/3$. There are many option, and we invite the reader to explore as well.

4.4 Lempel-Ziv Poincaré sections for fixed b

A commonn method of analyzing dynamical systems is plotting a trajectory's return to a Poincaré section. In some cases one can also use it to prove the existence of a limit cycle or chaotic behavior. When it comes to visualization, one can only plot a handful of different trajectories in a Poincaré section before the image becomes too busy and illegible, so we see the details of a selection of trajectories and not the full picture.

We propose to apply a similar procedure for Poincaré sections as in the previous section: fix a value for b, and sample initial conditions on the Poincaré section, and compute LZC for each. If the resolution and depth of iteration is high enough. In such a way, we achieve a general picture of the dynamics.

Recall, the Poincaré section is parametrized by two angles θ and φ, the former is for the position, and the latter for the direction of the velocity. We fixed the speed to be 1. We only consider $\theta \in [-\pi/4, \pi/4]$, that is, only the right "side" of the circle S_{out}. We do not lose information doing this, since system eq. (1) has 4-fold rotational symmetry due to the lattice arrangement of the magnetic discs. The lattice is invariant under all square symmetries, but since the magnetic field always turns trajectories to the right, we cannot use reflections to further shrink the window to plot.

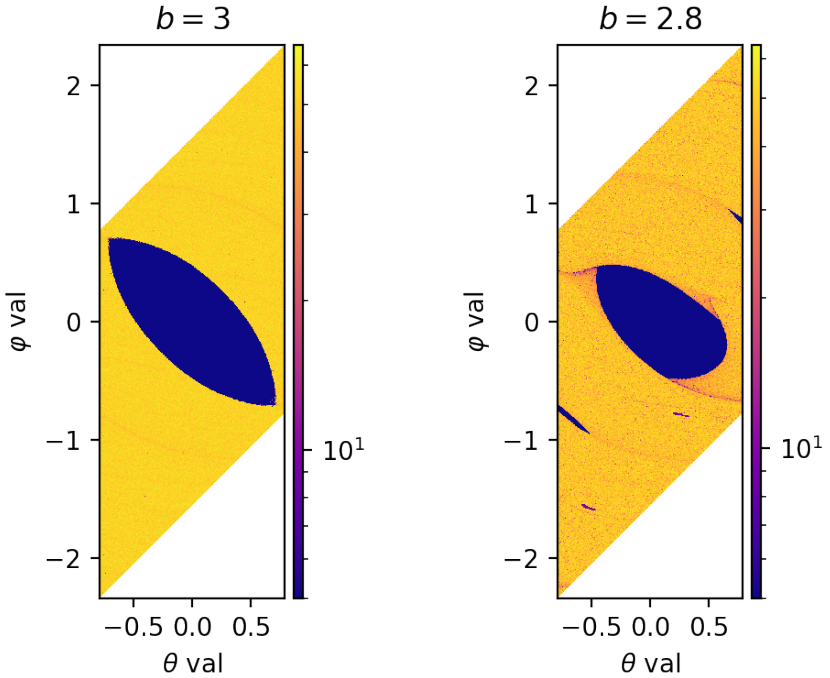

(a) (b)

Figure 9: With the same approach as in the previous section, we analyze a piece of the Poincaré section for fixed values of b. When $b = 3$ we see one large low complexity region, while for $b = 2.8$, we see something similar but deformed. The appearance of more little regions suggests a bifurcation might have occured.

In fig. 9a, we again focus on $b = 3$, which has the periodic trajectory fig. 4a. The dynamics appears to be simple, there is a large region of quasi-periodic trajectories around $(\theta, \varphi) = (0, 0)$, and the rest is uniformly high LZC. In fig. 9b, we perturb $b = 2.8$, the stable region from 9a changed shape, it is smaller, and there are now more noticeable artifacts along the boundary. Besides that, we see new stable regions: one larger, and two small. The two small ones likely belong to the same quasi-periodic trajectory, while the larger region belongs to its own. Looking back at fig. 13b, since there we had $b = 2.805$, we see indicated a periodic trajectory along the bottom edge of the Poincaré section. Here, we expect a similar trajectory, perhaps slightly perturbed. It's interesting to note that in fig. 9a we see faint streaks in the same spots where there are stable regions in fig. 9b. We conjecture that the patterns and streaks in the noise suggest a nearby bifurcation.

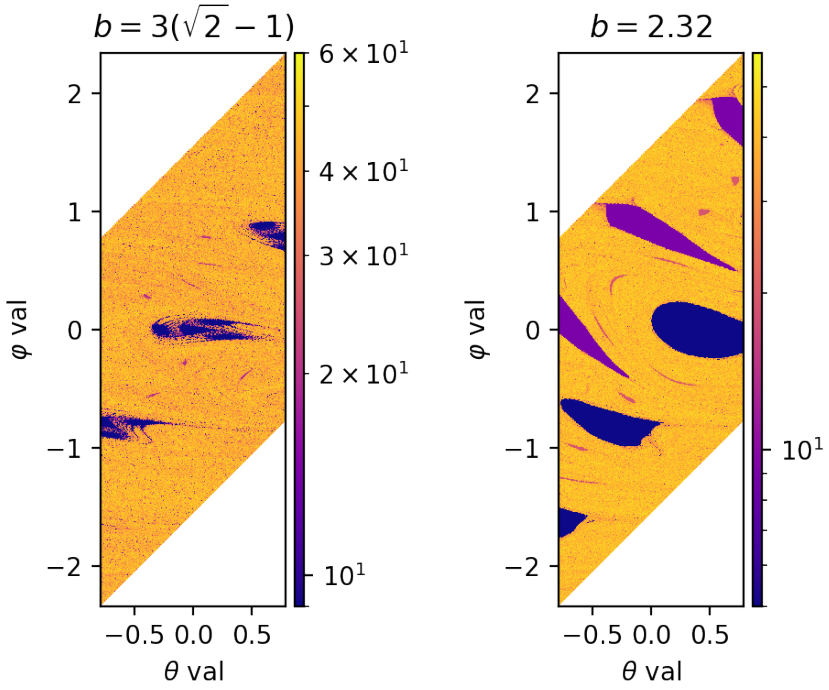

(a) (b)

Figure 10: We look at more values of b to illustrate the range of different structures. For $b = 3(\sqrt{2} - 1)$ we see some rotating fractal-like structures, and for $b = 2.32$ we see regions of varying shape and complexity.

In fig. 10a we plot the same data except $b \approx 3(\sqrt{2} - 1)$, corresponding to fig. 4c. The size of the blue regions is about the same, so there should relate to the same quasi-periodic orbit. What's different in this case is the pronounced teardrop with fractal-like structure. If we were to iterate deeper, it looks like the fractal branches would connect to make 4 disjoint blue blobs. Around the main big region, we see smaller red specks, suggesting another quasi-periodic trajectory that we didn't expect before.

In fig. 10b, $b = 2.32$, the kind of quasi-periodicity here should be similar to 13a, 12a, and 11b. It's plausible there are 3 different quasi-periodic regions here, since you can separate the blobs easily into three sets: blue along the bottom, purple along the top, and small red in between.

4.5 Checking for quasi-periodicity

In the previous two sections we described the "landscape" of the dynamics of (1) and determined regions with low complexity, signalling that potentially for initial conditions and parameters in those regions we can expect quasi-periodic behavior. In this section we pick points from the low LZC regions in fig. 7, 6 and fig. 9, 10 to check what the corresponding trajectories look like. Each trajectory is visualized to a depth of 2000 iterations of the Poincaré map, unless stated otherwise.

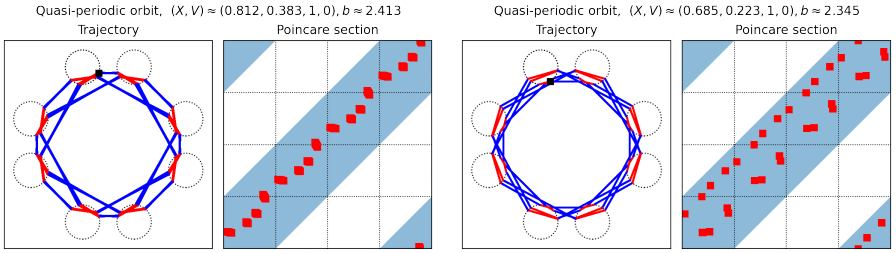

(a) (b)

Figure 11: Picking initial conditions from the low complexity regions in fig. 6 we find immediately some quasi-periodic behavior. The above two examples seem similar, yet the right one has a doubled period compared to the left.

Figure 11a and 11b are interesting, since they have a similar shape. The latter seems to be a "doubled" version of the former, and not a perturbation, since even after 2000 iterations the trajectory of 11b does not change, e.g., it does not smear like in the case of 4b.

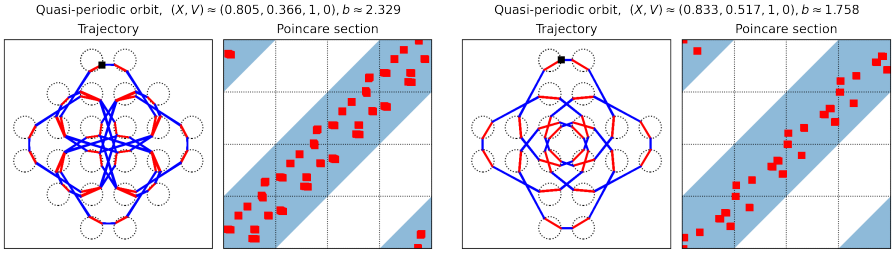

(a) (b)

Figure 12: Examples of quasi-periodic trajectories that we would not have found without the LZC analysis in the previous section.

Figure 12a and 12b are surprisingly complex patterns, and unlike the rest of the examples, involve many discs in the plane

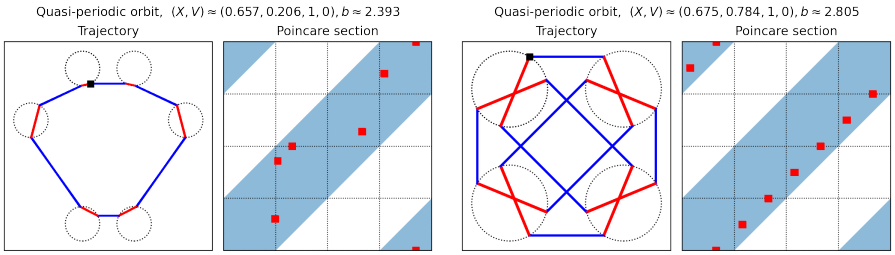

(a) (b)

Figure 13: The trajectory on the left is the first we fould that only has one reflectional symmetry, unlike the other examples that have many symmetries. The trajectory on the right does not demonstrate anything new but we included it anyway.

So far, we have seen trajectories that have lots of symmetries, the first to break this is 13a with a bottom-heavy hexagon. It would be interesting to see if there are other polygon, for example triangles or pentagons. Figure 13b does not illustrate anything new, we included it because it is aesthetically pleasing.

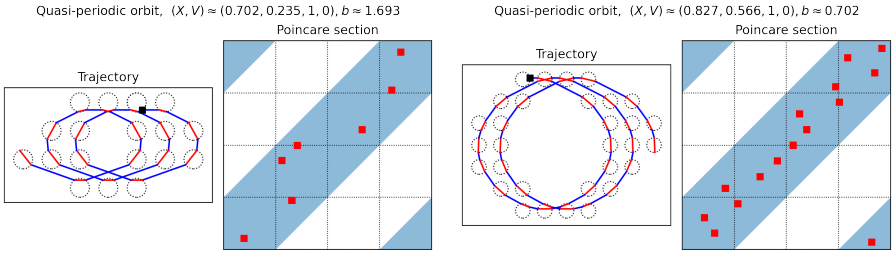

(a) (b)

Figure 14: The above trajectories are examples that are quasi-periodic in $\mathbb{T}^2$ but are wandering in $\mathbb{R}^2$, illustrating how the magnetic Lorentz gas and magnetic Sinai billiard are qualitatively different.

In fig. 14a and 14b we have the first examples of trajectories that wander in the plane but are quasi-periodic in the torus. It seems that these patterns arise in between values of b that produce trajectories as in fig. 15, that is, as b decreases, the radii of the circles in the pattern increases, and if, in a specific way, the circle does not close, you can still see repetition.

The last 15a - 15d are examples with values of b relatively small compared to the rest. The lower the value of b, the closer the shape resembles a circle, which is in line with what we had seen using KAM. We have not found any intricate patterns for low values of b.

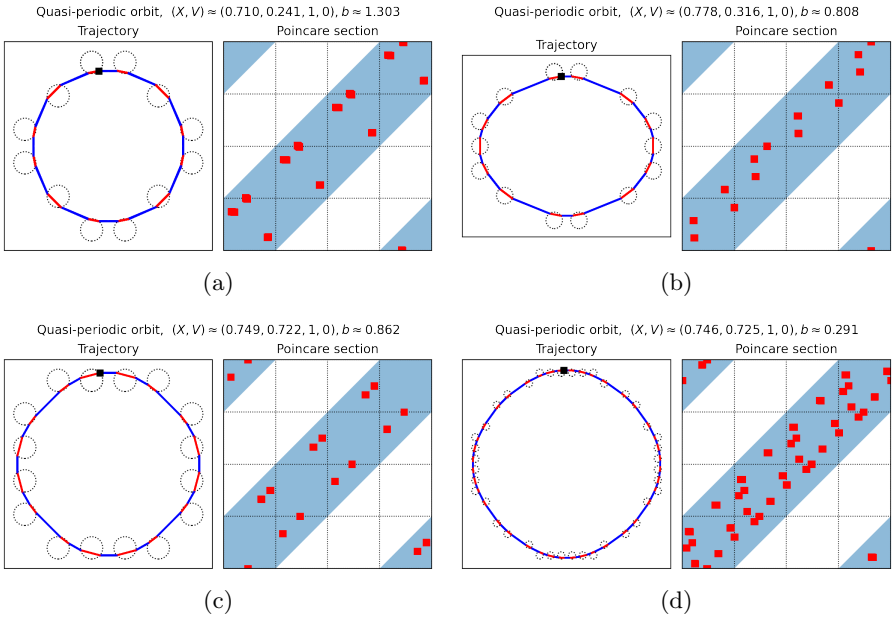

Figure 15: These trajectories are evidence supporting the claims that (1) can be viewed as a perturbation of a uniform magnetic field in the plane.

We see that in this simple system there is interesting dynamics with varying levels of complexity. It is safe to say that at least some of these would be hard to find by hand, and would be feasible only with some numerics and a measure of complexity for determining good candidates. We now construct the Poincaré section S_{in} and after that we outline the methods we used to obtain these quasi-periodic trajectories.

5 Conclusion

We began by introducing the magnetic Sinai billiard, and the relevant material for KAM theory, stability analysis, symbolic dynamics and Lempel-Ziv complexity. With that we analyzed the dynamics of the system which helped us characterize two modes: a weak mode, and an intermediate mode.

The weak mode is characterized by a small value for the field strength b. Using the KAM theorem, we reasoned that for $b \approx 0$, the dynamics on $\mathbb{T}^2$ can be interpretted as a perturbation of free motion on $\mathbb{T}^2$. Furthermore, we noticed that if $b \not\approx 0$ but still not too large, then the dynamics can be interpretted as a perturbation of a uniform field with strength $\hat{b} \approx \pi R^2 b$ where R is the radius of the magnetic disc. The value of π was predicted theoretically and substantiated with numerical evidence.

The idea to study (1) as a perturbation of free motion on $\mathbb{T}^2$ was considered from the very start of the thesis. Originally, we did not intend to consider the uniform field in the plane, we only stumbled upon the idea when developing the code and figures. Wrapping the trajectories to the unit square $[0,1]^2$ seemed like extra work at the time, and, knowing the numerical sensitivity of the system, it was decided that unwrapping trajectories to the plane would help visualization and debugging of code. Only once we unwrapped the trajectories did we notice that they had a circular shape. In short, a change of perspective showed another facet of the problem we didn't expect.

Continuing with the intermediate mode, it is characterized by a wide range of b for which we can find both seemingly ergodic components of the phase-space and stable components. Using the Lempel-Ziv complexity, we discovered many quasi-periodic trajectories that we would not have found otherwise. The Lempel-Ziv complexity proved to be a useful and efficient tool for detecting quasi-periodic trajectories among disorganised trajectories.

Studying the intermediate mode came with its own challenges as well, it was expected to be a difficult problem from the start. We wanted to try symbolic dynamics, yet were overwhelmed with both the restrictions and possibilities presented. For example, we suspected that S_{out} was a Poincaré section early on but only proved the fact quite late into the research. It also seemed that the literature on Markov partitions and semi-conjugacies for extracting symbolic dynamics was too restrictive and difficult to determine in our case. A preliminary analysis had indicated that some choices of b gave rise to more complicated behavior, and it was not clear how to capture it all with one Markov partition. Eventually, we switched to a more signal-processing like approach using the Lempel-Ziv complexity. Once that happened, there was no need for semi-conjugacies and compatible partitions, so restrictions were loosened. Still, we needed to generate symbols in some way and the options we considered seemed artificial. Before settling on the alphabet $(\mathbb{Z}^2)^{\mathbb{N}}$, for a while we used $\{N, S, E, W\}$, for North, South, East, and West. We then tracked how a trajectory interacted with the boundary of $[0,1]^2$, if it crossed one of the lines $y = 1$, $y = 0$, $x = 1$, $x = 0$ before wrapping to the other side of $[0,1]^2$, then we recorded the symbol N, S, E or W, respectively. The results we found using this alphabet were similar to what we have now, however there were extra artifacts. One possible cause for this could be the accumulation of redundant information, for example, if we know the trajectory leaves the disc at $(1/2, 1/2)$ and enters the one at $(1 + 1/2, 1 + 1/2)$, then either EN or NE could be recorded. In general,

for any jump, this alphabet accumulates possibly long sequences of 2 symbols where a number of different permutations could occur. So, we introduced unnecessary noise this way. The alphabet $(\mathbb{Z}^2)^{\mathbb{N}}$ avoids introducing this noise but since it is infinite, it's not ideal either, yet it still produced interesting results.

We covered a lot of ground while studying (1), considered a few options and found a few dead ends. We believe this is a good first step at a better understanding of this system. Having said this, there are still questions that can be explored further.

5.1 Further questions

Despite the work that we've done, there is still much to ask about this system and its dynamics.

We posed conjecture 1. We had used KAM theory to motivate it but further theoretical study probably requires different methods. From the perspective of numerics, one can make the applicable range of values of R and b more precise.

The use of `Sympy` greatly helped to compute eigenvalues of the Poincaré map. There were limitations on the complexity of the expressions that could be computed in a reasonable length of time. This makes it a less attractive method of analysis, despite the sophisticated expressions it can produce. So, to make it more viable, one could either try different software or try to find another simpler expression for P_o which could speed up the process.

On the same note, we had only determined eigenvalue pairs $\lambda_\pm$ that either both had $|\lambda_\pm| = 1$ or $|\lambda_+| < 1$ and $|\lambda_-| > 1$. So, we did not find periodic points of the Poincaré map that had both $|\lambda_\pm| < 1$. Can we find trajectories that are difinitively stable or even asymptotically stable?

When analyzing the LZC plots, we only considered a handful of trajectories, and only one or two from each region of low complexity. It would be interesting to study more deeply a single such region to see if these regions are as homogeneous as they seem. Due to LZC we have a general picture but the detail is lost, in fig. 9a there is a large region of low complexity surrounding $(\theta, \varphi) = (0, 0)$. However, we only considered trajectories near $(0, 0)$, and not farther away. We noticed but did not report that the point $(0.695, -0.695)$ falls within the region but has a period of 20 iterations. Using LZC we could not detect this long period, since the trajectory was trapped between the same 4 magnetic bumps. This is evidence that, indeed, the low complexity regions contain more to study.

Building on the previous point, one shortcoming of our analysis using LZC was the naive choice of alphabet and corresponding map to the shift space. One could search for a better alphabet, one that is more efficient (possibly finite) and one that would reveal more detail with LZC.

We discussed weak and intermediate field strengths b and did not consider $b \gg 1/R$. It's expected that the dynamics of the system will be ergodic almost everywhere for large values of b, though this still needs to be explored.

Another thing we noticed but did not address is that for large b, the system behaves similar to a Levy flight. A Levy flight [CMKG08] is a type of random walk in which the step lengths have a *stable distribution*.

A stable distribution is characterized by a slowly decaying tail which allows extremely long step lengths to occur more frequently than for example in *Brownian motion* where the step lengths are distributed normally. Due to this, Levy flights exhibit clustering, as can be seen in fig. 16. The size of the clusters and

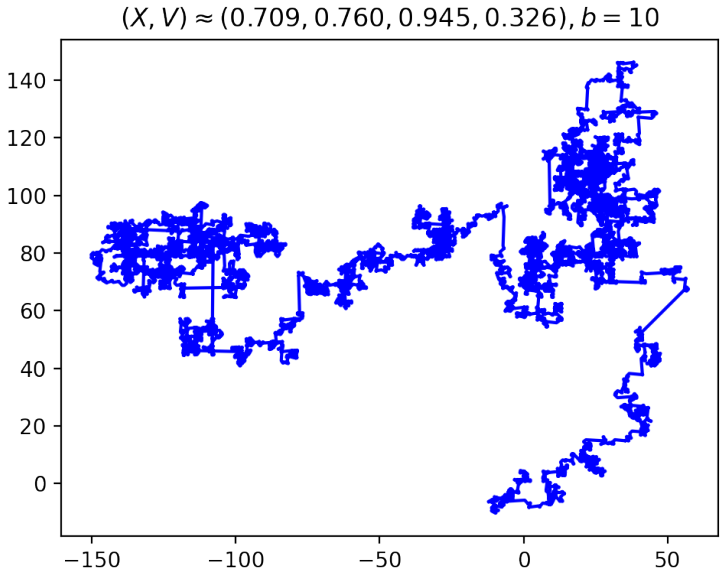

Figure 16: A trajectory computed to 10000 iterations. The result resembles a Levy flight, since there are clusters of short range motion along with long jumps.

the frequency of the jumps seem to depend on both b and R, the radius of the magnetic discs.

Levy flights are used to model many real world processes, for example, chemical processes, spread of infection diseases, and stock option strategies, so understanding (1) from this perspective can prove useful.

5.2 Acknowledgements

I would like to thank my supervisors who inspired and helped me to finish the thesis, and my family and friends who cared for me and reminded me to not make a mountain from a mole hill. I would also like to thank the individuals in the mathematical community whose writing styles are compatible with my type of comprehension, I have not met you personally but I feel like I know you.

References

[CMKG08] A. V. Chechkin, R. Metzler, J. Klafter, and V. Yu. Gonchar. *Introduction to the Theory of Lévy Flights*, chapter 5, pages 129–162. John Wiley & Sons, Ltd, 2008. https://onlinelibrary.wiley.com/doi/abs/10.1002/9783527622979.ch5.

[Coo93] I. D. Coope. Circle fitting by linear and nonlinear least squares. *Journal of Optimization Theory and Applications*, 76:381–388, Feb 1993. https://doi.org/10.1007/BF00939613.

[DL91] V. Donnay and C. Liverani. Potentials on the two-torus for which the hamiltonian flow is ergodic. *Communications in Mathematical Physics*, pages 267 – 302, 1991. https://doi.org/10.1007/BF02098044.

[Eva98] L. C. Evans. *Partial Differential Equations*. American Mathematics Society, 1998. Providence, RI.

[Gas21] S. Gasiorek. On the dynamics of inverse magnetic billiards. *Nonlinearity*, 34(3):1503–1524, mar 2021. https://doi.org/10.1088%2F1361-6544%2Fabe2f1.

[HSD13] M. W. Hirsch, S. T. Smale, and R. L. Devaney. *Differential equations, dynamical systems, and an introduction to chaos*. Pure and Applied Mathematics (Academic Press), 60. Elsevier, Academic Press, 3 edition, 2012;2013.

[Kna18] A. Knauf. *Mathematical Physics: Classical Mechanics*. Springer Berlin, Heidelberg, mar 2018. https://doi.org/10.1007/978-3-662-55774-7.

[KS87] F. Kaspar and H. G. Schuster. Easily calculable measure for the complexity of spatiotemporal patterns. *Physical review. A, General physics*, 36 2:842–848, 1987.

[KS17] A. Knauf and M. Seri. Symbolic dynamics of magnetic bumps. *Regular and Chaotic Dynamics*, 22(4):448–454, jul 2017. https://doi.org/10.1134%2Fs1560354717040074.

[LSIC04] S. J. Lee, S. Souma, G. Ihm, and K. J. Chang. Magnetic quantum dots and magnetic edge states. *Physics Reports*, 394(1):1–40, 2004.

[LZ76] A. Lempel and J. Ziv. On the complexity of finite sequences. *IEEE Transactions on Information Theory*, 22(1):75–81, January 1976.

[Pö82] J. Pöschel. Integrability of hamiltonian systems on cantor sets. *Communications on Pure and Applied Mathematics*, 35(5):653–696, 1982. https://onlinelibrary.wiley.com/doi/abs/10.1002/cpa.3160350504.

[Ras90] S. N. Rasband. *Chaotic dynamics of nonlinear systems*. Dover edition, 1990.

[Ser22] M. Seri. *Hamiltonian Mechanics*. AMS Open Math Notes, mar 2022. https://www.ams.org/open-math-notes/omn-view-listing?listingId=110861.

[Sil23] A. Silvans. Complex Dynamics of Magnetic Billiards in a 2-Torus CODE, October 2023. https://zenodo.org/doi/10.5281/zenodo.10030237.

[Sin63] Y. G. Sinai. On the foundations of the ergodic hypothesis for a dynamical system of statistical mechanics. *Dokl. Akad. Nauk SSSR*, 153:1261–1264, 1963. http://mi.mathnet.ru/dan28929.